TECHNICAL UNIVERSITY OF CRETE
SCHOOL OF ELECTRONIC AND COMPUTER ENGINEERING
TELECOMMUNICATIONS DIVISION

# Channel Coding and Detection for Increased Range Bistatic Scatter Radio

by

Panos N. Alevizos

A THESIS SUBMITTED IN PARTIAL FULFILLMENT OF
THE REQUIREMENTS FOR THE MASTER OF SCIENCE OF

ELECTRONIC AND COMPUTER ENGINEERING

October 2014

THESIS COMMITTEE

Associate Professor Aggelos Bletsas, *Thesis Supervisor*
Associate Professor George N. Karystinos
Associate Professor Antonios Deligiannakis

# Abstract

Scatter radio, i.e communication by means of reflection, has emerged as a potential key-enabling technology for ultra low-cost, large-scale, ubiquitous sensor networking. This work jointly studies noncoherent detection and channel coding for scatter radio networks, with the ultimate goal to further extend communication range, compared to prior art. Specifically, this work focuses on frequency shift keying modulation (FSK) in bistatic scatter radio architectures, where carrier emitter is dislocated from the software defined radio receiver (SDR). FSK is ideal for the power limited regime and allows for simple, frequency division multiple access (FDMA) of simultaneously operating receiver-less sensors.

A novel composite hypothesis testing decoding rule is derived for noncoherent channel-encoded FSK, in bistatic scatter radio architectures. Such decoding rule is evaluated with short block length channel codes; the latter offer ultra-low encoding complexity, and thus, they are appropriate for resource-constraint scatter radio sensors. Reed-Muller and BCH codes are studied, due to their strong algebraic structure. It is shown that the proposed decoding scheme achieves high diversity order through interleaving. Extensive simulations under Rician fading scenarios include the impact of carrier frequency offset estimation errors, channel coherence time and interleaving depth. Closed-form performance analysis is also provided. Theoretical analysis for maximum likelihood coherent detection and decoding in on-off keying modulation (OOK) is also presented. Furthermore, experimental measurements are conducted outdoors, with a commodity SDR reader and custom scatter radio sensor. Sensor-to-reader ranges up to 134 meters are experimentally demonstrated with omnidirectional antennas and 13 dBm (20 milliWatt) transmission power. Coded setup offered 10 additional meters range extension compared to the state-of-the-art uncoded noncoherent detection.

As a result, this thesis provided a simple solution that could further leverage the adoption of scatter radio in large-scale, ultra low-cost wireless sensor networks.

# Acknowledgements

First of all I would like to thank my family for their unconditional love and for their endless support.

I would like to express my sincerest thanks to my advisor Aggelos Bletsas, an excellent professor and researcher who provided me all the guidance I needed. His encouragement, his accurate remarks and his patience opened my way in the world of research, which I now adore.

Many thanks also go to my thesis committee, who graciously agreed to serve on my committee.

Special thanks go to professors Aggelos Bletsas, Athanasios P. Liavas, Georgios N. Karystinos and N. Sidiropoulos for their valuable contribution in my knowledge regarding telecommunication aspects.

Many thanks to all my adorable friends for their support and the unforgettable moments that we have lived together.

Finally, I would like to express my deepest thanks to my girlfriend, Georgia, who provided the greatest support and encouragement. She has always been there for me and ensured that I stay on balance.

*In memory of my grandparents.*

# Table of Contents

## Appendices

# List of Figures

# List of Abbreviations

| | |
|---|---|
| WSN | wireless sensor networks |
| RF | radio frequency |
| SDR | software-defined radio |
| RFID | radio frequency identification |
| CFO | carrier frequency offset |
| ML | maximum likelihood |
| pdf | probability density function |
| SPA | sum-product algorithm |
| RM | Reed Muller |
| BCH | Bose Chaudhuri Hocquenghem |

# Notation

| | |
|---|---|
| $x$ | a variable |
| $\mathbf{x}$ | a vector |
| $\mathbf{A}$ | a matrix |
| $\mathbf{A}^\top$ | transpose of matrix $\mathbf{A}$ |
| $\mathbf{A}^\mathrm{H}$ | conjugate transpose (hermitian) of matrix $\mathbf{A}$ |
| $\mathbf{I}_n$ | $n \times n$ identity matrix |
| $\lvert\mathcal{C}\rvert$ | the cardinality of a set $\mathcal{C}$ |
| $\lvert\lvert\mathbf{x}\rvert\rvert_p$ | the $p$ norm of a vector $\mathbf{x}$ |
| $\mathbb{R}$ | the set of real numbers |
| $\mathbb{C}$ | the set of complex numbers |
| $\mathbb{N}$ | the set of natural numbers |
| $f_{\mathbf{y}\lvert\mathbf{x}}(\mathbf{y}\lvert\mathbf{x})$ | a conditional pdf of random vector $\mathbf{y}$ given the vector $\mathbf{x}$ |
| $\mathbf{x} \sim \mathcal{N}(\boldsymbol{\mu}, \boldsymbol{\Sigma})$ | the random vector $\mathbf{x}$ follows multivariate Gaussian distribution with mean $\boldsymbol{\mu}$ and covariance matrix $\boldsymbol{\Sigma}$ |
| $\mathbf{x} \sim \mathcal{CN}(\boldsymbol{\mu}, \boldsymbol{\Sigma})$ | the complex random vector $\mathbf{x}$ follows multivariate complex Gaussian distribution with mean $\boldsymbol{\mu}$ and covariance matrix $\boldsymbol{\Sigma}$ |
| $\mathbb{B}$ | the set of binary numbers |
| $\mathbb{F}_q$ | the $q-$ary field |
| $\arg\max_{\mathbf{x}}\{f(\mathbf{x})\}$ | the argument that maximizes $f(\mathbf{x})$ |

A vector $\mathbf{x}$ of $n$ elements will be row-wisely denoted either as $\mathbf{x}^\top = [x_1, x_2, \ldots, x_n]$ or as $\mathbf{x}^\top = [x_1\ x_2\ \ldots\ x_n]$.

# Chapter 1

# Introduction

## 1.1 Extended Range Sensing

The need of ubiquitous environmental sensing has given rise to the utilization of large-scale wireless sensor networks (WSNs). Ideally, hundreds of sensors are placed in a large geographical area sensing time-dependent environmental variables (such as soil humidity, soil moisture, temperature) gathering the sensed information towards a central unit.

The existing commercial WSN equipment utilizes radios that incorporate complex active radio frequency (RF) components such as amplifiers, mixers, or high quality filters [2]. This type of RF components increase significantly the total monetary cost as well as the overall energy consumption per sensor node. As WSN become denser the use of such type of RF front-ends becomes prohibitive. Therefore, under relative stringent budget constraints and restricted energy resources, conventional WSN technology cannot offer ultra-high scalability environmental sensing.

## 1.2 Scatter Radio and Options for Range Extension

The idea of scatter radio is based on communication by means of reflection [3]. The main principle of such communication is that a carrier wave illuminates a RF tag sensor which terminates its antenna load according to the data to be transmitted. The induced signal's amplitude and/or phase depend on the current antenna load. In doing so, the incident signal is modulated and scattered back at the carrier frequency. In such framework the receiver also known as reader downconverts, demodulates and processes the backscattered information signal from tag.

Scatter radio has been extensively utilized in commercial radio frequency identification (RFID) systems for supply chain monitoring, object tracking, inventory control and plenty of other applications. Current research tends to employ scatter radio in wireless sensing applications (e.g. [4–7]), where the variable to be sensed alters the physical properties of an antenna; such alteration can be "read" through the signal reflected from the tag/sensor

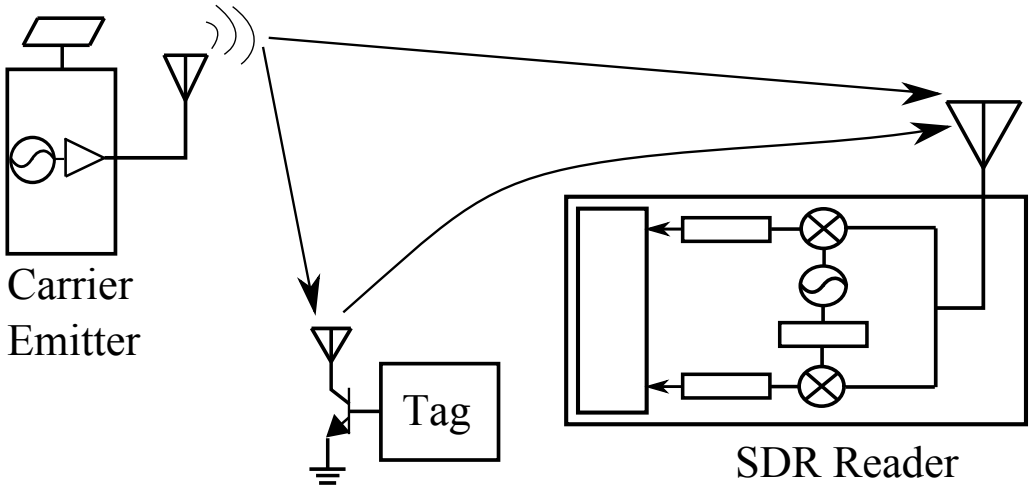


Figure 1.1: Bistatic scatter radio architecture: carrier emitter is dislocated from SDR reader. RF tag modulates the incident signal from carrier emitter which is scattered towards the SDR reader.

antenna and scattered back towards a software defined radio (SDR) reader. The benefit of such approach relies on the fact that the sensors/tags consist of simpler RF components, practically, consisting of a single RF transistor switch. In doing so, low monetary cost and low energy requirements can be obtained, giving rise to dense, cost-effective, large-scale sensor deployments.

Existing scatter radio sensing testbeds usually utilize commercial RFID readers and passive (batterry-less) tags/sensors. Relevant literature employees monostatic architectures where the reader box consists of both the transmit antenna that generates the carrier wave and the receive antenna which demodulates the reflected signal from the tags [4, 5, 8]. However, monostatic architectures suffer from round-trip path loss; specifically, SNR at the receiver drops with the fourth power of reader-to-tag distance [9], or the eighth power of the distance, for a two-ray propagation model [10].

Related work considers passive tags that require energy harvesting to power their electronics [5, 7, 8]. However, passive tags in conjunction with monostatic architectures offer limited communication ranges, on the order of few meters. This fact renders the utilization of passive tags an unsuitable option for increased sensing range applications.

In an effort to increase communication range, prior work has employed energy-assisted (i.e. *semi-passive*) tags, e.g. through the use of a battery [4] or a joint solar-radio frequency harvesting source [11]. It is noted that such tags continue to employ reflection rather than active transmission. Towards that direction work in [4] proposed a monostatic

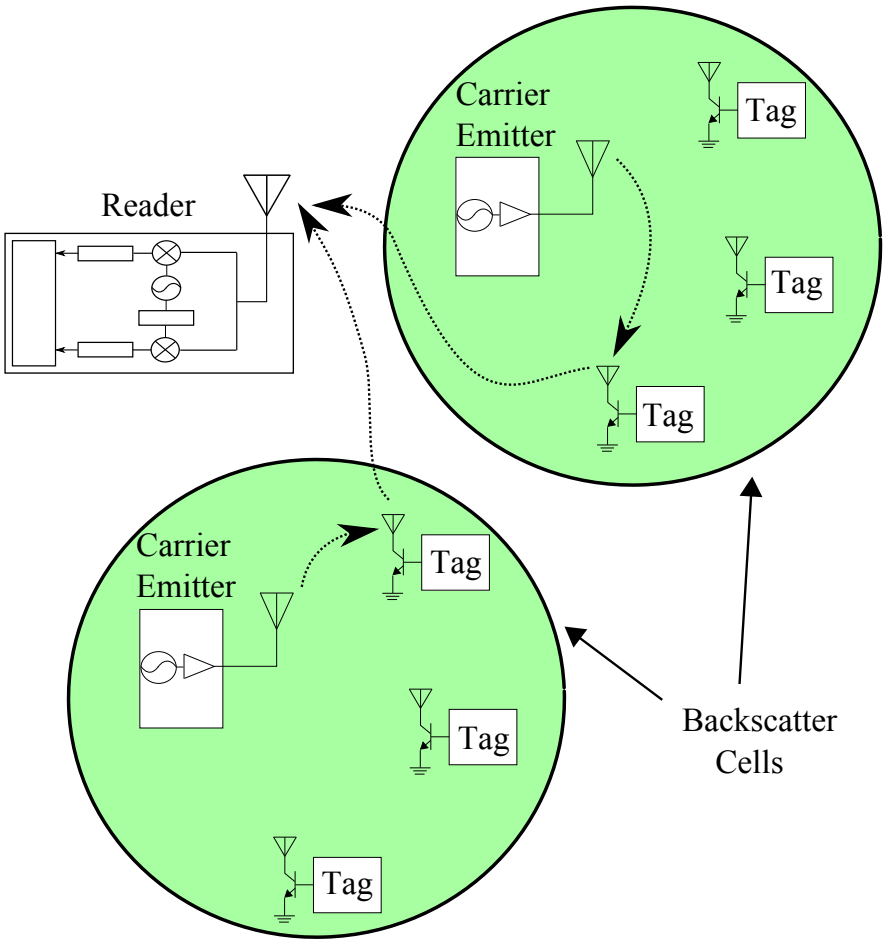


Figure 1.2: Bistatic scatter radio WSN: several ultra low-cost emitters, possibly powered through energy-harvesting techniques, can be stochastically placed in the field to illuminate multiple tag/sensors. A single SDR reader gathers the scattered information from the tags for further processing. Thus, flexible, ultra low-cost, large scale WSN topologies can be defined.

SDR reader, with battery-assisted tags and proposed detection algorithms for noncoherent minimum shift keying (MSK) modulation at the tags; the latter is ideal for the power-limited (low signal-to-noise-ratio (SNR)) regime, and allows for simple frequency division multiple access of simultaneously operating receiver-less tags [12].

Work in [13] proposed a *bistatic* scatter radio architecture, where carrier emitter and SDR receiver are dislocated (Fig. 1.1), derived the overall signal model and analyzed non-coherent detection algorithms for on-off keying modulation (OOK) (typically used in commercial RFID systems), as well as frequency-shift keying modulation (FSK) tailored to the bistatic setup. The basic idea in [13] is that *several* ultra low-cost emitters, possibly

powered through energy-harvesting techniques, can be stochastically placed in the field to illuminate multiple tag/sensors; thus, the probability of an emitter to be placed relatively close to a tag increases, offering potential link budget gains (Fig. 1.2). Using a commodity relatively-low cost SDR reader and no channel coding, experimental ranges on the order of 100 meters were demonstrated with the specific noncoherent detectors. It is noted that the system model adopted from [13], has been extensively verified experimentally [6, 14–17].

An additional approach towards range maximization relies on the use of channel codes (i.e error-correction coding). In the context of channel coding the *encoder* introduces redundancy on the transmitted information which is exploited by the *decoder* in order to increase the reliability of reception. This comes at the cost of reduction in transmission rate. Shannon, in his seminal paper [18], showed that the transmission rate does not need to go to zero in order to achieve reliable communication. Instead, any rate below the channel capacity (which depends solely on the channel) can offer reliable communication, provided that the codeword length tends to infinity. Another outstanding treatment related with channel coding can be found in [19].

From a practical viewpoint, the limited tag processing and storage capabilities impose stringent constraints on the block length of the utilized codes in scatter radio communication. Specifically, codes with a) short codeword length and b) low-complexity encoding, appropriate for resource-constrained tags/sensors should be utilized. Relevant literature related with channel coding in the context of bistatic scatter radio can be found in [1], where coherent FSK modulation is studied and maximum likelihood (ML) detection and decoding is offered. The authors proposed small code block length cyclic codes due to their inherent low space complexity encoding. Ranges up to 150 meters are experimentally demonstrated. Related work with channel coding tailored to the bistatic setup of [13] can be found in [20], where the authors proposed heuristic noncoherent decoding rule and achieved ranges up to 134 meters.

## 1.3 Thesis Contribution

The contribution of this thesis is summarized in the following bullets:

- A complete derivation of scatter radio signal model from the communication perspective is offered for FSK and OOK. The thesis completes the work in [13] and derives the baseband representation of the signal model accounting all communication parameters.

- Extremely important quantities in bistatic scatter radio link, such as instantaneous/average received SNR and instantaneous/average transmit CSR are defined and completely clarified, in order to efficiently design and analyze the performance of any transmission/reception scheme.
- A complete reference on possible inherent difficulties in bistatic scatter radio link is provided. Moreover, options to encounter such intractabilities are presented.
- For noncoherent FSK modulation the following are developed:
  - Composite hypothesis testing detection, which does not depend on channel characteristics. The specific hypothesis testing rule is equivalent with square-law detector.
  - ML detection when no fading is assumed (deterministic link attenuation).
  - Analytical closed form expression for the bit error rate (BER) performance of noncoherent square-law detector in the case where each link suffers from Rayleigh fading.
  - Novel composite hypothesis testing decoding rule which admits a very simple linear optimization problem.
- For coherent OOK modulation the following are developed:
  - Derivation of coherent OOK modulation with accurate ultra-low complexity ML channel parameter estimation.
  - ML detector along with its analytical performance (for Rayleigh fading).
  - ML decoder rule with or without interleaving technique.
- Extensive simulations that illustrate the impact of several communication parameters (CFO mismatch, interleaving depth, coherence time, type of fading) on the overall BER performance.
- Experimental validation of noncoherent coding in bistatic scatter radio FSK. Tag-to-reader ranges up to 134 meters are experimentally demonstrated, while BER reduction (or range increase), on the order of 10 additional meters (or more) compared to the uncoded case, with 20 miliwatts of carrier power, without directional antennas.

## 1.4 Thesis Outline

The thesis is organized as follows: Chapter 2 describes the system model for both FSK and OOK and introduces the inherent difficulties of bistatic scatter radio link. Chapter 3 presents channel coding technique to further increase tag–reader communication range. Chapters 4 and 5 offer the receiving schemes designed for noncoherent FSK and coherent OOK, respectively, and through simulations provide insight on how communication parameters affect their BER performance. Chapter 6 presents experimental results regarding noncoherent FSK modulation where coded setup offered range extension of 10 additional meters compared to the prior art. Thesis is concluded at Chapter 7.

# Chapter 2

# Problem Statement and System Model

## 2.1 System Model

The bistatic scatter radio architecture is employed, with a carrier emitter, a sensor tag and a software-defined radio (SDR) reader (Fig. 2.1) [13]; the emitter transmits a carrier at ultra-high frequency (UHF), illuminating a tag. The latter modulates the received carrier by terminating its antenna between two different loads (for binary modulations) and thus, the incident (at the tag) sinusoid wave is reflected with changed phase and amplitude; those two parameters depend on the tag antenna load that is selected each time.

Frequency non-selective (flat) fading is assumed (due to the relatively small communication bandwidth and relatively small channel delay spread), where for a duration of channel coherence time, $T_{\text{coh}}$, the *baseband* complex channel impulse response for each of three links depicted in Fig. 2.1 is given by

$$h_l(t) = h_l = a_l \, \mathsf{e}^{-\mathrm{j}\phi_l}, \; l \in \{\text{CR}, \text{CT}, \text{TR}\},$$

where $a_{\text{CR}}, a_{\text{CT}}, a_{\text{TR}} \in \mathbb{R}_+$ denote the channel attenuation parameters of the corresponding links and $\phi_{\text{CR}}, \phi_{\text{CT}}, \phi_{\text{TR}} \in [0, 2\pi)$ stand for the respective phases due to signal propagation delay. The channel impulse response parameters are *independent* of each other and change independently every $T_{\text{coh}}$.

Carrier emitter transmits a continuous sinusoid wave at carrier frequency $F_c$, its complex baseband equivalent is given by

$$c(t) = \sqrt{2P_C} \, \mathsf{e}^{-\mathrm{j}(2\pi\Delta F t + \Delta\phi)},$$

where $P_C$ is the carrier transmitting power at passband, $\Delta F$ and $\Delta\phi$ model the carrier frequency and carrier phase offset between carrier emitter and SDR reader, respectively.

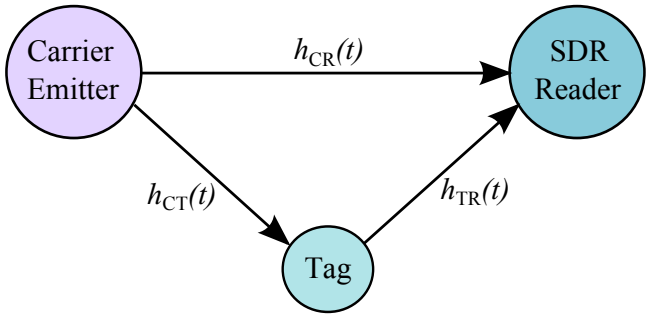


Figure 2.1: Bistatic architecture system model.

$\Delta\phi$ is modeled as random variable with uniform distribution in $[0, 2\pi)$, i.e. $\Delta\phi \sim \mathcal{U}[0, 2\pi)$. Tag is illuminated by the sinusoid wave $c(t)$, attenuated and rotated due to the channel gain $h_{\mathrm{CT}}$.

The reflected waveform is further attenuated by a parameter $s$, which depends on the tag inherent scattering efficiency and can be considered constant for a block of few bits (e.g. one transmission packet). More specifically, if we consider two tag load values, the baseband scattered waveform can be written as [13]

$$\begin{aligned} x(t) &= s\left(\left(A_s - \frac{\Gamma_0 + \Gamma_1}{2}\right) + \frac{\Gamma_0 - \Gamma_1}{2} u_i(t)\right) a_{\mathrm{CT}}\ \mathsf{e}^{-\mathsf{j}\phi_{\mathrm{CT}}} c(t) \\ &= s\left(v_0 + \frac{\Gamma_0 - \Gamma_1}{2} u_i(t)\right) a_{\mathrm{CT}} \mathsf{e}^{-\mathsf{j}\phi_{\mathrm{CT}}} c(t),\ i \in \mathbb{B}. \end{aligned} \tag{2.1}$$

$u_i(t)$ corresponds to modulation waveform of bit $i \in \mathbb{B} \triangleq \{0, 1\}$ and differs according to what modulation is utilized. $v_0$ is a DC constant that depends on the tag antenna structural mode $A_s$ [21] and the tag reflection coefficients $\Gamma_0, \Gamma_1$.

Thus, for duration $T$ of a single bit, the received baseband signal at the SDR reader is given by the superposition of the carrier emitter sinusoid and the backscattered tag signal through channels $h_{\mathrm{CR}}(t)$ and $h_{\mathrm{TR}}(t)$

$$\begin{aligned} y(t) &= a_{\mathrm{CR}}\ \mathsf{e}^{-\mathsf{j}\phi_{\mathrm{CR}}} c(t) + a_{\mathrm{TR}}\ \mathsf{e}^{-\mathsf{j}\phi_{\mathrm{TR}}} x(t) + n(t) \\ &= \sqrt{2P_C}\left(a_{\mathrm{CR}} \mathsf{e}^{-\mathsf{j}\phi_{\mathrm{CR}}} + a_{\mathrm{CT}} a_{\mathrm{TR}} \mathsf{e}^{-\mathsf{j}(\phi_{\mathrm{CT}} + \phi_{\mathrm{TR}})} s\left(v_0 + \frac{\Gamma_0 - \Gamma_1}{2} u_i(t)\right)\right) \mathsf{e}^{-\mathsf{j}(2\pi\Delta F t + \Delta\phi)} + n(t). \end{aligned} \tag{2.2}$$

Parameters

$$\begin{aligned}
\phi_0 &= \phi_{\mathrm{CR}} + \Delta\phi, \\
\phi_2 &= \phi_{\mathrm{CT}} + \phi_{\mathrm{TR}} + \Delta\phi, \\
\phi_1 &= \phi_2 + \underline{/\Gamma_0 - \Gamma_1}, \\
m_0 &= \sqrt{2P_C}a_{\mathrm{CR}}, \\
m_1 &= \sqrt{2P_c}a_{\mathrm{CT}}a_{\mathrm{TR}}s\frac{|\Gamma_0 - \Gamma_1|}{2}, \\
m_2 &= \sqrt{2P_c}a_{\mathrm{CT}}a_{\mathrm{TR}}sv_0,
\end{aligned}$$

are utilized for simplified notation. Therefore, by utilizing the above abbreviations, after some elementary calculations Eq. (2.2) can be written as

$$y(t) = \Big(m_0\mathsf{e}^{-\mathrm{j}\phi_0} + m_2\mathsf{e}^{-\mathrm{j}\phi_2} + m_1\mathsf{e}^{-\mathrm{j}\phi_1}u_i(t)\Big)\mathsf{e}^{-\mathrm{j}2\pi\Delta Ft} + n(t), \quad i \in \mathbb{B}. \tag{2.3}$$

$n(t)$ is a baseband complex Gaussian random process which stands for the thermal noise at receiver.

Carrier frequency offset (CFO) $\Delta F$ can be directly estimated using the Fast Fourier transform (FFT) and periodogram-based techniques [13]. CFO estimation depends on all terms of Eq. (2.3), including those where no tag information is modulated.[1] After CFO estimation and compensation, the received signal is sampled with sampling period $T_s$ and the baseband signal samples for a bit duration $T$ is given by:[2]

$$y[k] \triangleq y(kT_s) = \underbrace{\big(m_0\mathsf{e}^{-\mathrm{j}\phi_0} + m_2\mathsf{e}^{-\mathrm{j}\phi_2}\big)}_{\text{DC term}} + m_1\mathsf{e}^{-\mathrm{j}\phi_1}u_i(kT_s) + n[k], \quad i \in \mathbb{B}. \tag{2.4}$$

with $n[k] = n(kT_s) \sim \mathcal{CN}(0, 2\sigma_n^2)$ denoting the $k$th noise sample from random noise process $n(t)$. The power spectral density of baseband complex Gaussian process $n(t)$ is given by

$$S_{nn}(F) = \begin{cases} \frac{N_0}{2}, & |F| \le W \\ 0, & \text{otherwise}, \end{cases}$$

i.e., each noise sample has power $\mathbb{E}[|n[k]|^2] = 2\sigma_n^2 = N_0W$.

The instantaneous transmit carrier-to-signal ratio (CSR) is defined as the instantaneous

[1] Therefore, tag-dependent parameters such as $A_s$, typically overlooked in the literature, do play important role in the CFO estimation step [13].

[2] The receiver utilizes either energy synchronization or preamble-based correlation synchronization in order to find the start of the packet. Hereafter, it is assumed perfect synchronization.

power ratio between the transmitted carrier power and the *reflected* tag signal power. More specifically:

$$\mathrm{CSR}(a_{\mathrm{CT}}) \triangleq \frac{P_C}{P_T(a_{\mathrm{CT}})}.$$

$P_T(a_{\mathrm{CT}})$ is the instantaneous tag reflected (i.e. transmitted) power that depends on random amplitude $a_{\mathrm{CT}}$. The average tag reflected power is given by:

$$\mathtt{P_T} = \mathop{\mathbb{E}}_{a_{\mathrm{CT}}} \left[ P_T(a_{\mathrm{CT}}) \right]. \tag{2.5}$$

The average transmit CSR, `CSR`, is defined as the ratio of the average carrier power and the average tag power, i.e.

$$\mathtt{CSR} \triangleq \frac{P_C}{\mathtt{P_T}}. \tag{2.6}$$

The instantaneous received signal-to-noise ratio (SNR) per bit is defined as

$$\mathrm{SNR}(a_{\mathrm{CT}}, a_{\mathrm{TR}}) \triangleq \frac{P_T(a_{\mathrm{CT}})|a_{\mathrm{TR}}|^2}{2\sigma_n^2} L \tag{2.7}$$

whereas the average received SNR is

$$\mathtt{SNR} = \mathop{\mathbb{E}}_{a_{\mathrm{TR}}, a_{\mathrm{CT}}} \left[ \mathrm{SNR}(a_{\mathrm{CT}}, a_{\mathrm{TR}}) \right]. \tag{2.8}$$

It should be noted that the quantities $a_{\mathrm{TR}}$ and $a_{\mathrm{CT}}$ are positive real numbers and the magnitude square is equivalent with the square of the numbers. The magnitude operator is simply used by convention.

### 2.1.1 Frequency Shift Keying Modulation

In FSK modulation the tag modulates its information by switching the load at two distinct values (and thus, producing two distinct reflection coefficients $\Gamma_0$ and $\Gamma_1$) with different rates $F_0$ and $F_1$ ($F_0$ corresponding to bit "0" and $F_1$ to bit "1").[3] Modulation waveform $b_i(t)$ represents the fundamental frequency component of a 50% duty cycle square waveform

[3]Utilization of more than two loads was recently demonstrated in [22].

of frequency $F_i$ which may be written as [13]:[4]

$$u_i(t) = \frac{4}{\pi}\mathsf{cos}\big(2\pi F_i t + \Phi_i\big)\Pi_T(t),\ i \in \mathbb{B}, \tag{2.9}$$

where $\Pi_T(t)$ is the rectangular pulse of duration equal to bit period, $T$,

$$\Pi_T(t) \triangleq \begin{cases} 1, & 0 \le t < T, \\ 0, & \text{otherwise.} \end{cases}$$

$\Phi_i \sim \mathcal{U}[0, 2\pi]$ models the phase mismatch between the tag and the reader when bit $i \in \mathbb{B}$ is transmitted and is assumed that remains constant within a packet duration. Furthermore, it is assumed that $\Phi_0$ is independent of $\Phi_1$.

For FSK modulation the received digitalized signal of Eq. (2.4) is expressed ($i \in \mathbb{B}$)

$$y[k] \triangleq y(kT_s) = (m_0\mathsf{e}^{-\mathsf{j}\phi_0} + m_2\mathsf{e}^{-\mathsf{j}\phi_2}) + \frac{4}{\pi}m_1\mathsf{e}^{-\mathsf{j}\phi_1}\mathsf{cos}(2\pi F_i k T_s + \Phi_i)\Pi_L[k] + n[k]. \tag{2.10}$$

where $L \triangleq \frac{T}{T_s}$ is the oversampling factor. Notation $\Pi_L[k]$ stands for the oversampled version of $\Pi_T(t)$, i.e.

$$\Pi_L(k) \triangleq \begin{cases} 1, & k = 0, 1, \ldots, L-1 \\ 0, & \text{otherwise.} \end{cases}$$

The terms $m_0\mathsf{e}^{-\mathsf{j}\phi_0}$ and $m_2\mathsf{e}^{-\mathsf{j}\phi_2}$ do not contribute any information and can be eliminated with a DC-blocking filter. Thus, after DC-blocking the digital waveform can be written as ($i \in \mathbb{B}$)

$$\tilde{y}[k] = \tilde{m}_1\mathsf{e}^{-\mathsf{j}\phi_1}\mathsf{cos}(2\pi F_i k T_s + \Phi_i)\Pi_L[k] + n[k],$$

or equivalently, as follows ($i \in \mathbb{B}$)

$$\tilde{y}[k] = \frac{\tilde{m}_1}{2}\Big(\mathsf{e}^{\mathsf{j}(2\pi F_i k T_s + \Phi_i - \phi_1)} + \mathsf{e}^{-\mathsf{j}(2\pi F_i k T_s + \Phi_i + \phi_1)}\Big)\Pi_L[k] + n[k], \tag{2.11}$$

where we set $\tilde{m}_1 = \frac{4}{\pi}m_1$.

[4]It can be shown that the fundamental frequency component holds $\approx 80\%$ of the total power of the 50% duty cycle square pulse [4]. By including the rest harmonics, would at best, improve signal strength by 1 dB. Hence, the substantial additional cost and complexity associated with the wider bandwidth is not justified.

The instantaneous reflected power of tag for bistatic backscattered FSK is given by[5]

$$P_T(a_{\mathrm{CT}}) = \frac{|\Gamma_0 - \Gamma_1|^2}{4} \frac{16 s^2 P_C |a_{\mathrm{CT}}|^2}{\pi^2} = \frac{4 s^2 P_C |a_{\mathrm{CT}}|^2 |\Gamma_0 - \Gamma_1|^2}{\pi^2}. \tag{2.12}$$

If we use Eqs.(2.12) and (2.5), we obtain the average tag reflected power as

$$\mathtt{P_T} = \mathop{\mathbb{E}}_{a_{\mathrm{CT}}} \left[ |a_{\mathrm{CT}}|^2 \right] \frac{4 s^2 P_C |\Gamma_0 - \Gamma_1|^2}{\pi^2}. \tag{2.13}$$

If we combine Eqs. (2.6) and (2.13), we obtain the average transmit CSR, i.e.

$$\mathtt{CSR} = \frac{\pi^2}{|\Gamma_0 - \Gamma_1|^2 4 s^2 \mathop{\mathbb{E}}_{a_{CT}} [|a_{\mathrm{CT}}|^2]}$$

Finally if we use Eqs. (2.7), (2.8) and (2.13) we obtain the instantaneous and the average SNR, respectively,

$$\mathrm{SNR}(a_{\mathrm{CT}}, a_{\mathrm{TR}}) = \frac{2 |\Gamma_0 - \Gamma_1|^2 s^2 P_C}{\pi^2 \sigma_n^2} L |a_{\mathrm{CT}}|^2 |a_{\mathrm{TR}}|^2, \tag{2.14}$$

$$\mathtt{SNR} = \frac{2 |\Gamma_0 - \Gamma_1|^2 s^2 P_C}{\pi^2 \sigma_n^2} L \mathop{\mathbb{E}}_{a_{\mathrm{CT}}, a_{\mathrm{TR}}} \left[ |a_{\mathrm{CT}}|^2 |a_{\mathrm{TR}}|^2 \right]. \tag{2.15}$$

**Demodulation with Correlators**

The received signal of Eq. (2.11) is the sum of two complex exponentials with frequencies $\pm F_i$ and unknown phases $(\Phi_i - \phi_1)$ and $(-\Phi_i - \phi_1)$. If the orthogonality criterion of noncoherent FSK is satisfied, i.e. $|F_1 - F_0| = \frac{k}{T},\ k \in \mathbb{N}$, then any such 2 exponentials of frequencies $\pm F_0$ and $\pm F_1$ will be orthogonal.

It is noted that because the scatter radio tag modulation occurs directly at passband, two subcarriers appear for each frequency $F_i,\ i \in \mathbb{B}$. More specifically, the baseband waveform of Eq. (2.9) reveals that two subcarriers exist for each $F_i,\ i \in \mathbb{B}$ (Fig. 2.2), one at the positive semiaxis and one at the negative, which implies that 2 complex basis functions exist for each frequency $F_i,\ i \in \mathbb{B}$ (i.e. $\frac{1}{\sqrt{T}} \mathsf{e}^{-\mathrm{j}2\pi F_i t} \Pi_T(t), \frac{1}{\sqrt{T}} \mathsf{e}^{+\mathrm{j}2\pi F_i t} \Pi_T(t)$). This fact implies that classic FSK receiver offers a 3dB loss of information, due to the fact that the latter correlates only against frequencies $+F_i,\ i \in \mathbb{B}$ (Fig. 2.3), and thus, it is not suitable in bistatic scatter radio.

[5]The link from carrier emitter to SDR reader (CR) aggregates only DC offset to compound link emitter-tag-SDR reader. After the DC blocking its affection to the received signal is eliminated.

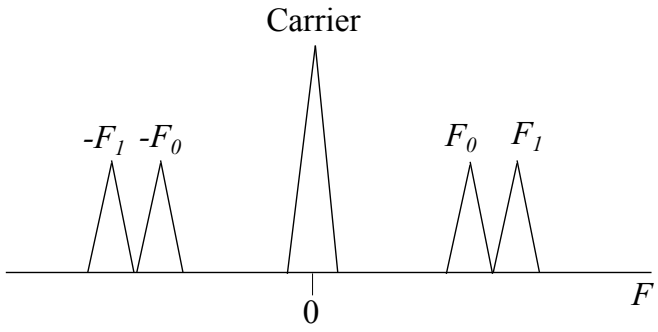


Figure 2.2: Complex baseband spectrum for bistatic scatter radio FSK. Two subcarrier per frequency exist in backscatter FSK.

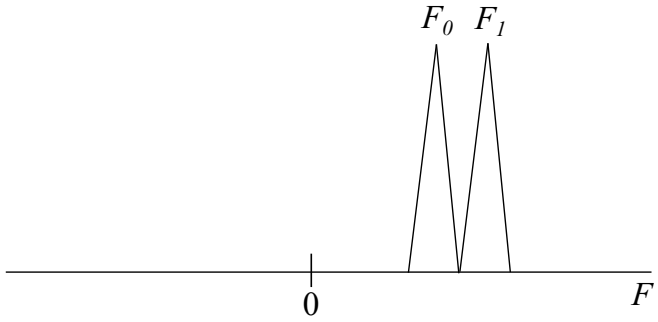


Figure 2.3: Complex baseband spectrum for classic FSK. Only one subcarrier exists per frequency.

For bistatic scatter radio FSK receiver a correlation demodulator can be utilized for each subfrequency $\pm F_0$ and $\pm F_1$, since it can exploit the orthogonality property and maximizes the received SNR. Specifically, for a bit duration $T$, a bank of demodulators processes the corresponding samples for each frequency $\pm F_0$ and $\pm F_1$ [13][6]

$$r_0^+ = \sum_{k=-\infty}^{+\infty} \tilde{y}[k] \left(\Pi_L[k] \mathsf{e}^{+\mathsf{j}2\pi F_0 k T_s}\right)^* = \sum_{k=0}^{L-1} \tilde{y}[k] \mathsf{e}^{-\mathsf{j}2\pi F_0 k T_s} = \frac{\tilde{m}_1}{2} \sum_{k=0}^{L-1} \mathsf{e}^{+\mathsf{j}(2\pi(F_i - F_0)kT_s + \Phi_i - \phi_1)} + n_0^+.$$

It is noted that $n_0^+ = \sum_{k=0}^{L-1} n[k] \mathsf{e}^{-\mathsf{j}2\pi F_0 k T_s}$ is the sum of $L$ independent complex Gaussians and thus, it follows complex Gaussian distribution with zero mean and variance $2\sigma_n^2 L$.

[6]Note that in theory correlation demodulator performs integration, however, in a practical system this is done by summation with relative high oversampling factor.

Similarly, the remaining correlator outputs are given by

$$r_0^- = \frac{\tilde{m}_1}{2}\sum_{k=0}^{L-1} \mathsf{e}^{-\mathsf{j}(2\pi(F_i-F_0)kT_s+\Phi_i+\phi_1)} + n_0^-,$$
$$r_1^+ = \frac{\tilde{m}_1}{2}\sum_{k=0}^{L-1} \mathsf{e}^{+\mathsf{j}(2\pi(F_i-F_1)kT_s+\Phi_i-\phi_1)} + n_1^+,$$
$$r_1^- = \frac{\tilde{m}_1}{2}\sum_{k=0}^{L-1} \mathsf{e}^{-\mathsf{j}(2\pi(F_i-F_1)kT_s+\Phi_i+\phi_1)} + n_1^-,$$

where $n_0^-, n_1^+, n_1^- \sim \mathcal{CN}(0, 2\sigma_n^2 L)$.

It is further noted that for $W \gg \frac{1}{T}$ and $W$ sufficiently larger than $F_i, i \in \mathbb{B}$, the orthogonal basis functions utilized here $\left\{\mathsf{e}^{+\mathsf{j}2\pi F_i t}\Pi_T(t), \mathsf{e}^{-\mathsf{j}2\pi F_i t}\Pi_T(t)\right\}_{i\in\mathbb{B}}$ can be considered limited within the $[-W, W]$ frequency band, since the Fourier transform functional of $\mathsf{e}^{\pm\mathsf{j}2\pi F_i t}\Pi_T(t)$, $\mathcal{F}\{\mathsf{e}^{\pm\mathsf{j}2\pi F_i t}\Pi_T(t)\}$, decays in frequency domain as $\mathsf{sinc}(\cdot)$ function with parameter $T$, i.e.,

$$\mathsf{sinc}(TF) = \frac{\mathsf{sin}(\pi TF)}{\pi TF}, \tag{2.16}$$

around $\pm F_i, i \in \mathbb{B}$. Therefore, since $n(t)$ is a complex baseband Gaussian random process with power spectral density $\frac{N_0}{2}$ in the $[-W, W]$ frequency band, its projections on an orthonormal basis (with bandwidth limited basis functions in $[-W, W]$) will offer i.i.d. zero-mean complex Gaussian components [23, 24].

When bit "1" is transmitted (i.e. frequency $F_1$ is utilized), the output from correlator is

$$r_0^+ = n_0^+, \qquad r_1^+ = \frac{\tilde{m}_1 L}{2}\mathsf{e}^{-\mathsf{j}\phi_1}\mathsf{e}^{+\mathsf{j}\Phi_1} + n_1^+,$$
$$r_0^- = n_0^-, \qquad r_1^- = \frac{\tilde{m}_1 L}{2}\mathsf{e}^{-\mathsf{j}\phi_1}\mathsf{e}^{-\mathsf{j}\Phi_1} + n_1^-,$$

whereas, when bit "0" is transmitted the output from correlator is

$$r_0^+ = \frac{\tilde{m}_1 L}{2}\mathsf{e}^{-\mathsf{j}\phi_1}\mathsf{e}^{+\mathsf{j}\Phi_0} + n_0^+, \qquad r_1^+ = n_1^+,$$
$$r_0^- = \frac{\tilde{m}_1 L}{2}\mathsf{e}^{-\mathsf{j}\phi_1}\mathsf{e}^{-\mathsf{j}\Phi_0} + n_0^-, \qquad r_1^- = n_1^-,$$

Let $\mathbf{r} = \left[r_0^+, r_0^-, r_1^+, r_1^-\right]^\top$ and $\mathbf{n} = \left[n_0^+, n_0^-, n_1^+, n_1^-\right]^\top$, then the discrete baseband equivalent

signal for a single bit period is obtained as

$$\mathbf{r} = \frac{\tilde{m}_1 L}{2} \mathsf{e}^{-\mathrm{j}\phi_1} \mathbf{s} \odot \begin{bmatrix} \mathsf{e}^{+\mathrm{j}\Phi_0} \\ \mathsf{e}^{-\mathrm{j}\Phi_0} \\ \mathsf{e}^{+\mathrm{j}\Phi_1} \\ \mathsf{e}^{-\mathrm{j}\Phi_1} \end{bmatrix} + \mathbf{n}, \quad \mathbf{s} \in \mathcal{S}_{\mathrm{FSK}}, \tag{2.17}$$

where from the independence of noise components we have that

$$\mathbf{n} \sim \mathcal{CN}(\mathbf{0}, 2\sigma_n^2 L \mathbf{I}_4). \tag{2.18}$$

Symbol $\odot$ denotes the Hadamard product (component-wise product), and $\mathcal{S}_{\mathrm{FSK}} \triangleq \{\mathbf{s}_0, \mathbf{s}_1\}$, where $\mathbf{s}_0 \triangleq [1,1,0,0]^\top$ and $\mathbf{s}_1 \triangleq [0,0,1,1]^\top$.

For a sequence of $N$ bits, the receiver after synchronization applies demodulation for each bit in the sequence, utilizing the basis functions at suitable time instants. The discrete baseband equivalent signal for a sequence of $N$ bits can be written as

$$\mathbf{r}_j = \frac{\tilde{m}_1 L}{2} \mathsf{e}^{-\mathrm{j}\phi_1} \mathbf{s}_j \odot \begin{bmatrix} \mathsf{e}^{+\mathrm{j}\Phi_0} \\ \mathsf{e}^{-\mathrm{j}\Phi_0} \\ \mathsf{e}^{+\mathrm{j}\Phi_1} \\ \mathsf{e}^{-\mathrm{j}\Phi_1} \end{bmatrix} + \mathbf{n}_j, \quad j = 1, \ldots, N, \quad \mathbf{s}_j \in \mathcal{S}_{\mathrm{FSK}}, \tag{2.19}$$

where $\mathbf{r}_j \triangleq \left[r_0^+(j), r_0^-(j), r_1^+(j), r_1^-(j)\right]^\top$ and $\mathbf{n}_j \triangleq \left[n_0^+(j), n_0^-(j), n_1^+(j), n_1^-(j)\right]^\top$, $j = 1, \ldots, N$.

### 2.1.2 On-Off Keying Modulation

In OOK modulation the tag load coefficient is set for a constant duration $T$ at $\Gamma_0$ for bit "0" and at $\Gamma_1$ for bit "1". Thus, the information is modulated at the amplitude of the signal. The modulation waveform for bistatic backscatter OOK is given by [13]

$$u_i(t) = x\Pi_T(t), \quad x \in \{-1, 1\},$$

where $u_0(t) = -\Pi_T(t)$ and $u_1(t) = \Pi_T(t)$, $\Pi_T(t)$ is defined as before, and $x$ denotes the transmitted symbol. The digitalized signal at SDR of Eq. (2.4) for OOK modulation is

given by

$$y[k] \triangleq y(kT_s) = \left(m_0 \mathsf{e}^{-\mathsf{j}\phi_0} + m_2 \mathsf{e}^{-\mathsf{j}\phi_2}\right) + m_1 \mathsf{e}^{-\mathsf{j}\phi_1} x \Pi_L[k] + n[k],\ x \in \{-1, 1\}, \tag{2.20}$$

In OOK modulation the terms $m_0\mathsf{e}^{-\mathsf{j}\phi_0}$ and $m_2\mathsf{e}^{-\mathsf{j}\phi_1}$ cannot be eliminated with a DC blocking filter because the signal is modulated at the amplitude. They must be firstly estimated with a known preamble bit sequence and then can be eliminated.

The instantaneous reflected power of tag for bistatic scatter radio OOK, without accounting the DC terms, is given by[7]

$$P_T(a_{\mathrm{CT}}) = 2s^2 P_C |a_{\mathrm{CT}}|^2 \frac{|\Gamma_0 - \Gamma_1|^2}{4} = \frac{s^2 P_C |a_{\mathrm{CT}}|^2 |\Gamma_0 - \Gamma_1|^2}{2}. \tag{2.21}$$

If we use Eqs. (2.5) and (2.21), we obtain the average tag reflected power as

$$\mathtt{P_T} = \mathop{\mathbb{E}}_{a_{\mathrm{CT}}} \left[|a_{\mathrm{CT}}|^2\right] \frac{s^2 P_C |\Gamma_0 - \Gamma_1|^2}{2}. \tag{2.22}$$

If we combine Eqs. (2.6) and (2.22) average transmit CSR is obtained

$$\mathtt{CSR} = \frac{2}{s^2 \mathop{\mathbb{E}}_{a_{\mathrm{CT}}} \left[|a_{\mathrm{CT}}|^2\right] |\Gamma_0 - \Gamma_1|^2}.$$

Finally, if we use Eqs. (2.7), (2.8) and (2.22), the instantaneous and the average received SNR for bistatic scatter radio OOK is, respectively, given by

$$\mathrm{SNR}(a_{\mathrm{CT}}, a_{\mathrm{TR}}) = \frac{s^2 P_C |\Gamma_0 - \Gamma_1|^2}{4\sigma_n^2} L |a_{\mathrm{CT}}|^2 |a_{\mathrm{TR}}|^2, \tag{2.23}$$

$$\mathtt{SNR} = \frac{s^2 P_C |\Gamma_0 - \Gamma_1|^2}{4\sigma_n^2} L \mathop{\mathbb{E}}_{a_{CT}, a_{\mathrm{TR}}} \left[|a_{\mathrm{CT}}|^2 |a_{\mathrm{TR}}|^2\right]. \tag{2.24}$$

### Demodulation with Matched Filtering

The optimal demodulator in OOK utilizes matched filtering to maximize the received SNR [23]. Thus, the received signal of Eq. (2.20) is matched filtered with square pulse $\Pi_L[k]$ and the filtered signal is sampled at the end of each symbol period. The discrete baseband

[7] The link from carrier emitter to SDR reader (CR) is not accounted in the calculation of the SNR because it only aggregates DC offset to compound link emitter-tag-SDR reader, which is the link of interest.

equivalent signal for a single bit period is given by

$$\begin{aligned} r &= \sum_{k=0}^{L-1} y[k]\Pi_L[L-1-k] = \sum_{k=0}^{L-1} y[k] \\ &= \sum_{k=0}^{L-1} \left(m_0 \mathsf{e}^{-\mathsf{j}\phi_0} + m_2 \mathsf{e}^{-\mathsf{j}\phi_2}\right) + m_1 \mathsf{e}^{-\mathsf{j}\phi_1} x \Pi_L[k] + n[k] \\ &= L\left(m_0 \mathsf{e}^{-\mathsf{j}\phi_0} + m_2 \mathsf{e}^{-\mathsf{j}\phi_2}\right) + L m_1 \mathsf{e}^{-\mathsf{j}\phi_1} x + \sum_{k=0}^{L-1} n[k], \quad x \in \{-1, +1\}. \end{aligned}$$

The above equation can be rewritten as

$$\begin{aligned} r &= L\left(m_0 \mathsf{e}^{-\mathsf{j}\phi_0} + m_2 \mathsf{e}^{-\mathsf{j}\phi_2} - m_1 \mathsf{e}^{-\mathsf{j}\phi_1}\right) + \tilde{x} 2 m_1 \mathsf{e}^{-\mathsf{j}\phi_1} L + \sum_{k=0}^{L-1} n[k] \\ &= A_{\mathrm{DC}} + \tilde{x}(2 m_1 \mathsf{e}^{-\mathsf{j}\phi_1} L) + n, \quad \tilde{x} \in \{0, 1\}, \end{aligned} \tag{2.25}$$

where

$$n \triangleq \sum_{k=0}^{L-1} n[k] \sim \mathcal{CN}(0, 2\sigma_n^2 L)$$

and we abbreviate the DC term of Eq. (2.25) as

$$A_{\mathrm{DC}} \triangleq L\left(m_0 \mathsf{e}^{-\mathsf{j}\phi_0} + m_2 \mathsf{e}^{-\mathsf{j}\phi_2} - m_1 \mathsf{e}^{-\mathsf{j}\phi_1}\right) \in \mathbb{C}$$

It is observed that the above baseband equivalent signal representation resembles to the OOK one.

For a sequence of $N$ bits, the receiver after synchronization applies matched filtering on the received waveform for a duration of $N$ bit periods, and thus, the discrete baseband equivalent for the block of $N$ bits can be expressed as

$$r_j = A_{\mathrm{DC}} + x_j(2 m_1 \mathsf{e}^{-\mathsf{j}\phi_1} L) + n_j, \quad j = 1, 2, \ldots, N, \quad x_j \in \{0, 1\}. \tag{2.26}$$

### 2.1.3 Conventions in Fading Process

In order to equate the transmission power with the average received power for each of three links, it is convenient to assume that the average fading power at each of three links is

unit, i.e. $\underset{a_l}{\mathbb{E}}\left[|a_l|^2\right] = 1,\ l \in \{\mathrm{CR}, \mathrm{CT}, \mathrm{TR}\}$. Hereafter, it will be assumed that the average fading power is 1. Consequently, for bistatic scatter radio FSK, the average received SNR is given by

$$\boxed{\mathtt{SNR} = \frac{2\left|\Gamma_0 - \Gamma_1\right|^2 s^2 P_C}{\pi^2 \sigma_n^2} L}, \tag{2.27}$$

whereas for bistatic scatter radio OOK the average received SNR is

$$\boxed{\mathtt{SNR} = \frac{s^2 P_C \left|\Gamma_0 - \Gamma_1\right|^2}{4\sigma_n^2} L}. \tag{2.28}$$

## 2.2 Inherent Difficulties in Bistatic Scatter Radio

The first problem in bistatic scatter radio link is that there exist 6 random parameters that are related to the corresponding links

$$\{a_l, \phi_l\},\ l \in \{\mathrm{CR}, \mathrm{CT}, \mathrm{TR}\},$$

that play important role on how to design the receivers for both modulation schemes. Especially in backscatter FSK there exist 2 more random parameters, which are the random phases $\Phi_0$ and $\Phi_1$. In both modulations the most common approach to facilitate the parameter estimation (coherent reception) or parameter elimination process (noncoherent reception) is to treat some subsets of parameters as compound hyperparameters that can be estimated or eliminated more easily, without losing in optimality. Chapters 4 and 5 discuss how to treat these random parameters in order to design efficient noncoherent and coherent receivers.

Secondly, the fact that the carrier emitter is dislocated from SDR reader leads to CFO mismatch between their local oscillators. The impact of CFO mismatch between carrier emitter and the SDR reader may lead to severe performance degradation in terms of bit error rate (BER). The most common way to estimate CFO is to assume that remains static within the packet duration, and then, to use FFT to find the frequency where the periodogram of the received packet is maximized. After the estimation of CFO the periodogram of the received packet is shifted to DC. It is noted that for ultra-low bitrate scenarios where the bit duration $T$ is relative hight, the CFO needs to be estimated with high precision, and thus high-frequency resolution must be employed for perodogram. This

requires a long processing time, which may be prohibitive in some scenarios. Chapters 4 and 5 quantify this performance degradation with several types of receiver setups. In OOK modulation the impact of CFO mismatch can be eliminated if the receiver instead of process the received samples, it processes the absolute value of the samples, which immediately eliminates the CFO mismatch. However, the latter scheme loses 3 dB BER performance than the conventional scheme due to the absolute operation (3 dB amplification of noise power). Chapter 5 presents trade-offs between these 2 schemes.

The most common problem in wireless links with flat fading is the effect of deep fading, i.e. when the useful received signal is buried under the noise floor. In such cases the received signal is much possible to not be detected or decoded properly. Specifically, the effect of deep fading occurs if the instantaneous received SNR is below 1. For instance, suppose that bistatic backscatter OOK modulation is utilized and assume that each link suffers from Rayleigh fading, i.e. $\{a_l\},\ l \in \{\mathrm{CT}, \mathrm{TR}\}$, are Rayleigh random variables (r.v.'s) with unit power ($\underset{a_l}{\mathbb{E}}\left[|a_l|^2\right] = 1,\ l \in \{\mathrm{CT}, \mathrm{TR}\}$). Their corresponding probability density function (pdf) is given by

$$f_{a_l}(x) = 2x\mathsf{e}^{-x^2},\ x \geq 0,\quad l \in \{\mathrm{CT}, \mathrm{TR}\}.$$

Then the deep fading event occurs if

$$\mathrm{SNR}(a_{\mathrm{CT}}, a_{\mathrm{TR}}) \leq 1 \Longleftrightarrow \frac{s^2 P_C \left|\Gamma_0 - \Gamma_1\right|^2}{4\sigma_n^2} L|a_{\mathrm{CT}}|^2|a_{\mathrm{TR}}|^2 \leq 1 \Longleftrightarrow \mathtt{SNR}|a_{\mathrm{CT}}|^2|a_{\mathrm{TR}}|^2 \leq 1.$$

The probability of deep fading is given by

$$\Pr\left(\mathtt{SNR}|a_{\mathrm{CT}}|^2|a_{\mathrm{TR}}|^2 \leq 1\right) = \Pr\left(a_{\mathrm{CT}}a_{\mathrm{TR}} \leq \sqrt{\frac{1}{\mathtt{SNR}}}\right).$$

In order to calculate this probability event in closed form, we must find the pdf of the product of the independent Rayleigh distributed r.v.'s $a_{\mathrm{CT}}, a_{\mathrm{TR}}$. Let $a \triangleq a_{\mathrm{CT}}a_{\mathrm{TR}}$, where $a_{\mathrm{CT}}$ and $a_{\mathrm{TR}}$ are independent. If we use Eq. (6-148) (pp. 302) in [25] the pdf of r.v. $a$ can

be obtained as

$$\begin{aligned} f_a(a) &= \int_0^{+\infty} \frac{1}{x} f_{a_{\mathrm{CT}}}(x) f_{a_{\mathrm{TR}}}\left(\frac{a}{x}\right) \mathsf{d}x \\ &= 4a \int_0^{+\infty} \frac{1}{x} \mathsf{e}^{-\left(x^2+\left(\frac{a}{x}\right)^2\right)} \mathsf{d}x \\ &= 4a\mathsf{K}_0(2a), \quad a \geq 0, \end{aligned} \tag{2.29}$$

where the last line is obtained from [26] (pp. 370), Eq. (3.478.4). $\mathsf{K}_\nu(x)$ stands for the second kind modified Bessel function of $\nu$th order and its definition can be found in Appendix (Eq. (A.7)). Therefore, the probability of deep fading is

$$\begin{aligned} \Pr\left(a \leq \sqrt{\frac{1}{\mathtt{SNR}}}\right) &= \int_0^{\sqrt{\frac{1}{\mathtt{SNR}}}} 4a\mathsf{K}_0(2a)\mathsf{d}a \\ &= 1 - \frac{2}{\sqrt{\mathtt{SNR}}}\mathsf{K}_1\left(\frac{2}{\sqrt{\mathtt{SNR}}}\right). \end{aligned} \tag{2.30}$$

On the other hand if we had utilized OOK modulation along with Marconi-type communicators (which radiate their own carrier during transmission) over a Rayleigh flat fading channel (i.e., there exists single link between transmitter-receiver; thus, r.v. $a$ would be Rayleigh distributed), then the probability of deep fading would be

$$\begin{aligned} \Pr\left(a \leq \sqrt{\frac{1}{\mathtt{SNR}}}\right) &= \int_0^{\sqrt{\frac{1}{\mathtt{SNR}}}} 2a\mathsf{e}^{-a^2}\mathsf{d}a \\ &= 1 - \mathsf{e}^{-\frac{1}{\mathtt{SNR}}}. \end{aligned} \tag{2.31}$$

Fig. 2.4 illustrates the probability of deep fading event as a function of the average received SNR, $\mathtt{SNR}$, with OOK modulation for a classic link and a bistatic backscatter (compound) link. It is assumed that both links suffer from Rayleigh fading. From Fig. 2.4 is observed that the probability of deep fading in classic link is smaller than bistatic backscatter link. This fact indicates that the event of deep fading occurs more frequently in bistatic scatter link. For instance, for probability of deep fading equal to $10^{-3}$, there is 10 dB gap between the two schemes. It is noted that the gap increases as the $\mathtt{SNR}$ increases.

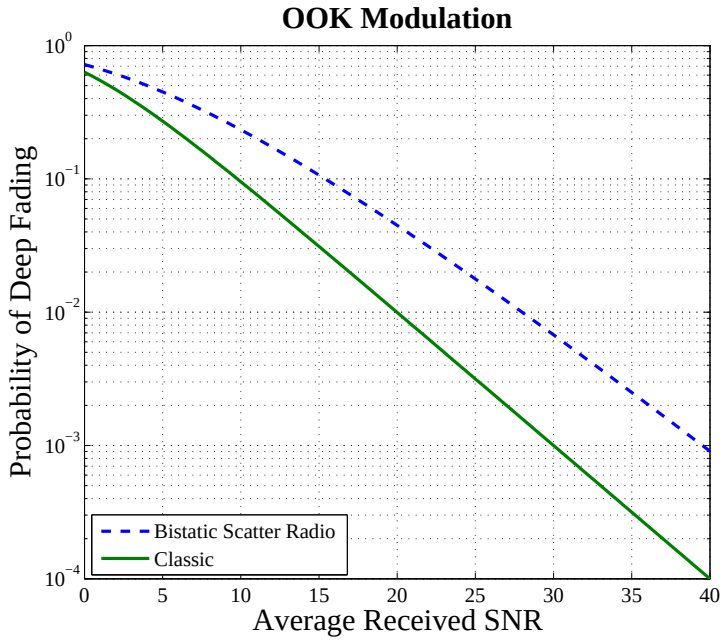


Figure 2.4: Probability of deep fading event as a function of average received SNR, `SNR`, for bistatic backscatter link and classic link in OOK.

# Chapter 3

# Options to Increase Range: Channel Coding

The most common way to increase the range of communication (or equivalently to decrease the probability of error for a given SNR) is to employ channel coding. The basic idea of channel coding is to introduce redundancy at the transmitted information in order to increase the minimum distance between possible outputs at the receiver, and thus, to decrease the probability of bit error. However, as the signal model changes, as well as the type of receiver varies (either coherent, or noncoherent) the decoding process must be carefully employed. The following subsections introduce the notion of channel encoding-decoding in bistatic scatter radio. In sequel, the idea of interleaving is presented, which aids to the problem of deep fading event when block codes with small block length are utilized. In this Chapter we focus solely on linear block codes over the binary field $\mathbb{F}_2 \equiv \mathbb{B}$.

## 3.1 Linear Block Codes for Bistatic Scatter Radio

### 3.1.1 Encoding of Linear Block Codes

The objective of encoding is to map with an one-to-one function a sequence of $K$ information bits to a sequence of $N \geq K$ coded bits. Since the simplest one-to-one function is a linear function, the encoder can be viewed as the linear function $f$ that maps a $K$ binary tuple to a $N$ binary tuple ($f : \mathbb{B}^K \mapsto \mathbb{B}^N$). Therefore, a linear block code $\mathcal{C}$ over the field $\mathbb{B}$, i.e. the set of all codewords, is a $K$ dimensional subspace of $\mathbb{B}^N$. There exist totally $|\mathbb{B}^K| = 2^K$ binary codewords. Since the dimension of $\mathcal{C}$ is $K$, there is a set of linearly independent vectors in $\mathbb{B}^N$ that form a basis for the code. Let $\mathbf{g}_1, \mathbf{g}_2, \ldots, \mathbf{g}_K \in \mathbb{B}^N$ be the

row basis vectors for $\mathcal{C}$; then the vectors are placed in a $K \times N$ generation matrix $\mathbf{G}$

$$\mathbf{G} \triangleq \begin{bmatrix} \mathbf{g}_1 \\ \mathbf{g}_2 \\ \vdots \\ \mathbf{g}_K \end{bmatrix}.$$

It is remarked that a binary $N$-tuple is a codeword of $\mathcal{C}$, if and only if there exists a binary $K$-tuple that can generate this $N$-tuple from $\mathbf{G}$, i.e.

$$\mathbf{c} \in \mathcal{C} \Longleftrightarrow \exists\ \mathbf{b} \in \mathbb{B}^K : \mathbf{c} = \mathbf{b}\mathbf{G}. \tag{3.1}$$

The ratio $r \triangleq \frac{K}{N}$ defines the rate of the code, while the minimum distance $d^{\mathcal{C}}_{\min}$ of a code $\mathcal{C}$ is the smallest Hamming weight (i.e. the number of non-zero components) of any codeword in $\mathcal{C}$, except the all zero codeword,

$$d^{\mathcal{C}}_{\min} \triangleq \min_{\mathbf{c} \in \mathcal{C} \setminus \{\mathbf{0}\}} w_{\mathrm{H}}(\mathbf{c}).$$

A code $\mathcal{C}$ is usually briefly described by the triplet $(N, K, d^{\mathcal{C}}_{\min})$ that affects its properties (in some cases the minimum distance of a code may not be specified and thus, the code will be abbreviated as an $(N, K)$ linear block code).

Therefore, encoding of $K$ bits that produce $N$ coded bits is performed at the tag by a simple multiplication with the generation matrix, as described by Eq. (3.1). The latter can be stored in the tag memory and can be directly implemented in ultra-low power, micro-controller unit (MCU)-based tags, as those used in [20]. The spatial complexity of this procedure is $\mathcal{O}(KN)$. The coded bits can be then reflected in the same way as with uncoded bits. Nevertheless, with resource-constrained tags, memory is not unlimited and $N, K$ should be both kept relatively small, as discussed below.

### 3.1.2 Soft-Decision Decoding of Linear Block Codes

The idea of decoding is to exploit the information redundancy that has been introduced by the encoder in order to increase the reliability of reception, at the cost of the reduction in transmission rate. Suppose that the receiver has applied the necessary signal processing (CFO estimation/compensation, synchronization, matched filtering or use of correlators, sampling, estimation of the random parameters in coherent setup) and obtains

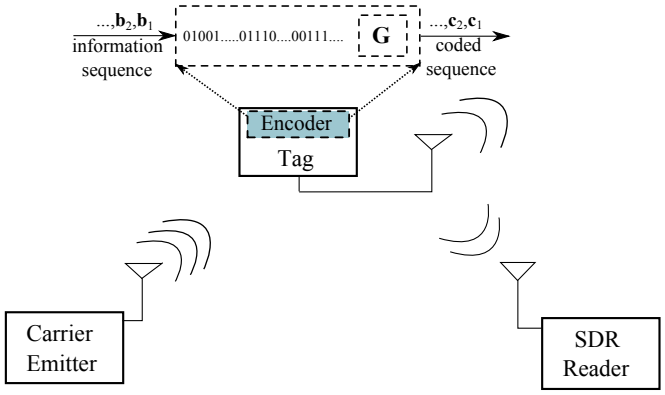


Figure 3.1: Encoding at the tag can be directly performed with a matrix multiplication. The latter is straightforward with ultra-low power micro-controller unit (MCU)-based tags.

a vector $\mathbf{y} = [\mathbf{y}_1, \mathbf{y}_2, \ldots, \mathbf{y}_N]^\top$ corresponding to the encoded transmitted bit sequence $\mathbf{c} = [c_1, c_2, \ldots, c_N] \in \mathbb{B}^N$. The objective of the decoder is to minimize the probability of error, or equivalently, to find the codeword that maximizes the likelihood of the observations given the transmitted encoded data sequence for equiprobable signaling (such a decoder is called ML soft-decision decoder). Let $\boldsymbol{\theta}_j$ be a vector of the random parameters for each modulation scheme, i.e. $j \in \{\text{OOK}, \text{FSK}\}$. More specifically,

$$\boldsymbol{\theta}_{\text{OOK}} = [a_{\text{CR}}, a_{\text{CT}}, a_{\text{TR}}, \phi_{\text{CR}}, \phi_{\text{CT}}, \phi_{\text{TR}}]^\top \in \mathbb{R}_+^3 \times [0, 2\pi)^3, \tag{3.2}$$

$$\boldsymbol{\theta}_{\text{FSK}} = [a_{\text{CT}}, a_{\text{TR}}, \phi_{\text{CT}}, \phi_{\text{TR}}, \Phi_0, \Phi_1]^\top \in \mathbb{R}_+^2 \times [0, 2\pi)^4. \tag{3.3}$$

According to what receiver is utilized the process of decoding changes. More specifically, given a code $\mathcal{C}$, the optimal noncoherent decoder finds the codeword $\mathbf{c} \in \mathcal{C}$ that maximizes the likelihood of observations $\mathbf{y}$ given the transmitted codeword $\mathbf{c}$ (assuming that all codewords are equiprobable), i.e.,

$$\mathbf{c}_{\text{ML}}^{\text{NC}} = \arg\max_{\mathbf{c}\in\mathcal{C}} f_{\mathbf{y}|\mathbf{c}}(\mathbf{y}|\mathbf{c}) = \arg\max_{\mathbf{c}\in\mathcal{C}} \mathop{\mathbb{E}}_{\boldsymbol{\theta}_j} \left[ f_{\mathbf{y}|\mathbf{c},\boldsymbol{\theta}_j}(\mathbf{y}|\mathbf{c}, \boldsymbol{\theta}_j) \right], \quad j \in \{\text{OOK}, \text{FSK}\}. \tag{3.4}$$

However, for OOK modulation the DC term must be estimated based on a preamble sequence instead of eliminated by means of expectation, because in the latter case the DC term accounts as extra noise with large variance after the expectation, and the performance of such scheme is very poor. As we will see in the subsequent chapter, efficient noncoherent composite hypothesis based decoder exists only for backscatter FSK modulation.

On the other hand, the optimal coherent decoder firstly estimates the random param-

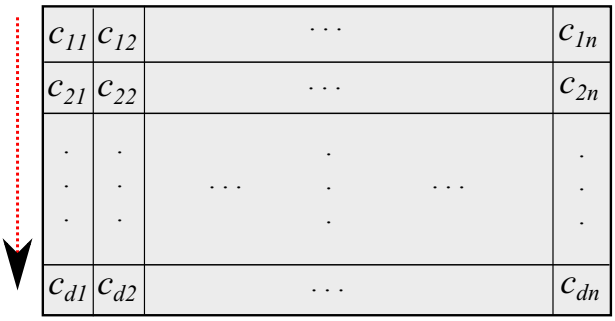


Figure 3.2: With interleaving, $d$ codewords are stored at the encoder and bits are transmitted column-wise. In that way, burst of errors due to fading affect bits of different codewords and not consecutive bit of the same codeword.

eters $\boldsymbol{\theta}_j$; let $\widehat{\boldsymbol{\theta}}_j$, $j \in \{\text{OOK}, \text{FSK}\}$ be an estimation of parameters. Then the coherent ML soft-decision decoder seeks the codeword $\mathbf{c} \in \mathcal{C}$ that maximizes the likelihood of observations $\mathbf{y}$ given the transmitted codeword $\mathbf{c}$ and the estimated parameters $\widehat{\boldsymbol{\theta}}_j$ (assuming that all codewords are equiprobable), i.e.,

$$\mathbf{c}_{\text{ML}}^{\text{C}} = \arg \max_{\mathbf{c} \in \mathcal{C}} f_{\mathbf{y}|\mathbf{c},\boldsymbol{\theta}_j}(\mathbf{y}|\mathbf{c}, \widehat{\boldsymbol{\theta}}_j), \quad j \in \{\text{OOK}, \text{FSK}\}. \tag{3.5}$$

The above optimization problems belong in class of $\mathcal{NP}-$hard problems [27]. However, there exist a computational efficient algorithm, known as sum-product algorithm (or belief propagation), that performs approximate ML decoding [27–29], and offers BER performance close to ML decoder's BER performance. In bistatic setup, where small block lengths are utilized due to resource constraint tags, the above decoding rules can be computed with low complexity.

## 3.2 Coding Gain with Interleaving

Section 2.2 showed that bistatic scatter radio link is more prone to deep fading events, where, errors usually occur in long bursts. The use of channel codes with small block length cannot overpass the deep fading event, due to their small bit error-correction capability.

In order to overpass this difficulty, the interleaving technique could be employed, in conjunction with linear block codes (of relatively small length). The transmitter stores a block of $d$ codewords for transmission and transmits the information column-wise, i.e. it transmits consecutively the first coded bit of each of the $d$ codewords and then the second bit of each of the $d$ codewords and so forth, until the $N$-th coded bit (Fig. 3.2). The

receiver stores $dN$ received symbols (in a $d \times N$ matrix) and performs decoding row-wise, i.e it decodes symbol sequences that correspond to actual codewords. With interleaving, the burst errors affect bits of different codewords rather than consecutive bits of the same codeword.

Parameter $d$ is the interleaving depth of the interleaver and it can be proved that as parameter $d$ increases, the linear block code can achieve diversity of order $d^{\mathcal{C}}_{\min}$ [23]. The choice of $d$ usually depends on the application and the corresponding channel coherence time $T_{\text{coh}}$. Despite its attractive flavor, the main drawback of this technique is the added delay at both transmitter and receiver side, since they must both store in their memory $d$ codewords before transmission or reception processing, respectively. The trade-off involved in interleaving is dependent on applications. In delay-tolerant systems deep interleaving is possible, and hence parameter $d$ can be kept relative hight. On the other hand, in delay-constrained systems, parameter $d$ must be kept relative small.

# Chapter 4

# Noncoherent Reception with Channel Coding in Bistatic Scatter Radio Link

When the unknown random channel parameters cannot be estimated at the SDR reader, or the tag cannot afford to send a preamble sequence (known to receiver), noncoherent reception schemes may be employed. The idea of noncoherent receiver adopts a Bayesian-based approach: elimination of random parameters using expectation. In OOK modulation, due to the term $A_{\mathrm{DC}}$ in Eq. (2.25), the expectation with respect to $A_{\mathrm{DC}}$ results in extra additive noise and the performance of such scheme is poor. Thus, in this section we solely focus on noncoherent FSK modulation in bistatic setup.

Before we proceed to noncoherent detection and decoding we must assume a probabilistic model for the random parameters.[1] For outdoors environments which are commonly encountered in WSN applications, there is probably strong line-of-site (LOS) signal for individual links and thus, it is customary to assume that the channel attenuation parameters are Rician-distributed random variables (r.v.s), [23], i.e.,

$$f_{a_l}(x) = 2(K_l+1)\; x\; \mathsf{e}^{-\left((K_l+1)\left(x^2+\frac{K_l}{K_l+1}\right)\right)}\; \mathsf{I}_0\Big(2x\sqrt{K_l(K_l+1)}\Big)\,,\; x \geq 0, \quad l \in \{\mathrm{CT}, \mathrm{TR}\}, \tag{4.1}$$

where the function $\mathsf{I}_\nu(x)$ is the first kind modified Bessel function of $\nu$th order and its definition can be found in Appendix (Eq. (A.6)). Parameter $K_l$ stands for the ratio between the power in the direct path and the power in the scattered paths of link $l \in \{\mathrm{CT}, \mathrm{TR}\}$. For the special case where $K_l = 0$ we obtain Rayleigh fading, while for $K_l = \infty$ we obtain no fading, i.e. fading parameters $a_{\mathrm{CT}}$ and $a_{\mathrm{TR}}$ are deterministic constants with $a_{\mathrm{CT}} = a_{\mathrm{TR}} = 1$. The impact of parameter $K_l$ in the BER performance will be discussed in Section 4.1.3.

[1] In FSK modulation, due to DC blocking operation the parameters $\{a_{\mathrm{CR}}, \phi_{\mathrm{CR}}\}$ do not contribute in either detection or decoding, and therefore can be omitted.

Parameters $\phi_{\mathrm{CT}}$ and $\phi_{\mathrm{TR}}$ are assumed to follow uniform distribution in $[0, 2\pi)$, i.e.

$$f_{\phi_l}(x) = \frac{1}{2\pi},\ x \in [0, 2\pi),\quad l \in \{\mathrm{CT}, \mathrm{TR}\}.$$

# 4.1 Noncoherent Processing in FSK

## 4.1.1 Noncoherent Detection

The SDR reader, after demodulation with correlators, possesses $N$ observation vectors $\mathbf{r}_j, j = 1, \ldots, N$ corresponding to $N$ transmitted bits $b_j, j = 1, \ldots, N$.[2] The optimal noncoherent symbol-by-symbol detection for the bistatic backscatter FSK (that minimizes the probability of bit error) is given by the following hypothesis testing (assuming equal priors for each hypothesis):

$$f_{\mathbf{r}_j|\mathbf{s}_0}(\mathbf{r}_j|\mathbf{s}_0) \underset{H_1}{\overset{H_0}{\gtrless}} f_{\mathbf{r}_j|\mathbf{s}_1}(\mathbf{r}_j|\mathbf{s}_1),\quad j = 1, \ldots, N, \tag{4.2}$$

where the hypothesis $H_0$ decides in favor of bit "0", whereas hypothesis $H_1$ decides in favor of bit "1", i.e. for any $j = 1, \ldots, N$, the optimal detector decides that bit "0" is sent, if $H_0$ is chosen, and bit "1" otherwise. Since symbol-by-symbol detection decides for each bit independently, it is convenient to focus in a single bit period, rather in the whole bit sequence, thus, omitting the subscripts, the problem can be written as

$$f_{\mathbf{r}|\mathbf{s}_0}(\mathbf{r}|\mathbf{s}_0) \underset{H_1}{\overset{H_0}{\gtrless}} f_{\mathbf{r}|\mathbf{s}_1}(\mathbf{r}|\mathbf{s}_1) \Longleftrightarrow f_{\mathbf{r}|H_0}(\mathbf{r}|H_0) \underset{H_1}{\overset{H_0}{\gtrless}} f_{\mathbf{r}|H_1}(\mathbf{r}|H_1). \tag{4.3}$$

**Can the ML Detector Be Derived for $K_l < \infty$?**

In order to apply ML detection the conditional pdfs $f_{\mathbf{r}|\mathbf{s}_0}(\mathbf{r}|\mathbf{s}_0)$ and $f_{\mathbf{r}|\mathbf{s}_1}(\mathbf{r}|\mathbf{s}_1)$ must be given in a closed form. In the following we will prove that $f_{\mathbf{r}|\mathbf{s}_i}(\mathbf{r}|\mathbf{s}_i),\ i \in \mathbb{B}$ do not admit closed form expression when $K_{\mathrm{CT}}, K_{\mathrm{CT}} \in [0, +\infty)$.

Firstly, it is remarked that $\mathsf{e}^{-\phi_1} = \mathsf{e}^{-\phi_1 + 2\pi}$, therefore, we do not lose in optimality if we assume that the random phases are within the interval $[0, 2\pi)$. If we recall that $\phi_1 = \phi_{\mathrm{CT}} + \phi_{\mathrm{TR}} + \Delta\phi + \underline{/\Gamma_0 - \Gamma_1}$, we obtain that $-\phi_1 \pmod{2\pi} \sim \mathcal{U}[0, 2\pi)$. Furthermore, we define $\theta_a \triangleq -\phi_1 + \Phi_0 \pmod{2\pi}$ and $\theta_b \triangleq -\phi_1 - \Phi_0 \pmod{2\pi}$ (or equivalently $\mathsf{e}^{-\mathsf{j}(\phi_1 - \Phi_0)} = \mathsf{e}^{\mathsf{j}\theta_a}$ and $\mathsf{e}^{-\mathsf{j}(\phi_1 + \Phi_0)} = \mathsf{e}^{\mathsf{j}\theta_b}$), where the phases $\phi_1$ and $\Phi_0$ are independent each other and thus,

[2] In this subsection no encoding of the information bits is assumed.

$\theta_a, \theta_b \sim \mathcal{U}[0, 2\pi)$. Then if we apply the same procedure with [25] (Example 6.31, pp. 313) in conjunction with modulo operation we obtain that

$$f_{\theta_a,\theta_b}(\theta_a, \theta_b) = \frac{1}{4\pi^2} = f_{\theta_a}(\theta_a) f_{\theta_b}(\theta_b), \quad \theta_a, \theta_b \in [0, 2\pi), \tag{4.4}$$

and thus, $\theta_a$ and $\theta_b$ are independent each other. Let

$$a \triangleq a_{\mathrm{CT}} a_{\mathrm{TR}},$$
$$\mu \triangleq \frac{\tilde{m}_1 L}{2a},$$

then the conditional pdf of the observation $\mathbf{r}$ given $H_0$ and the parameters is[3]

$$\begin{aligned} &f_{\mathbf{r}|H_0,a_{\mathrm{CT}},a_{\mathrm{TR}},\phi_{\mathrm{CT}},\phi_{\mathrm{TR}},\Phi_0}(\mathbf{r}|H_0, a_{\mathrm{CT}}, a_{\mathrm{TR}}, \phi_{\mathrm{CT}}, \phi_{\mathrm{TR}}, \Phi_0) = f_{\mathbf{r}|H_0,a_{\mathrm{CT}},a_{\mathrm{TR}},\theta_a,\theta_b}(\mathbf{r}|H_0, a_{\mathrm{CT}}, a_{\mathrm{TR}}, \theta_a, \theta_b) \\ &= f_{r_0^+|H_0,a_{\mathrm{CT}},a_{\mathrm{TR}},\theta_a}(r_0^+|H_0, a_{\mathrm{CT}}, a_{\mathrm{TR}}, \theta_a) f_{r_0^-|H_0,a_{\mathrm{CT}},a_{\mathrm{TR}},\theta_b}(r_0^-|H_0, a_{\mathrm{CT}}, a_{\mathrm{TR}}, \theta_b) \times \\ &\times f_{r_1^+|H_0}(r_1^+|H_0) f_{r_1^-|H_0}(r_1^-|H_0), \end{aligned} \tag{4.5}$$

where we utilized the conditional independence of $r_0^+, r_0^-, r_1^+, r_1^-$ given $H_0$ and the parameters $a_{\mathrm{CT}}, a_{\mathrm{TR}}, \theta_A$ and $\theta_B$. If we set $\sigma_A^2 = 2L\sigma_n^2$ then Eq.(4.5) can be written as follows

$$\text{Eq. (4.5)} = \frac{1}{\left(\pi\sigma_A^2\right)^4} \mathsf{e}^{-\frac{1}{\sigma_A^2}\left(|r_0^+|^2+|r_0^-|^2+|r_1^+|^2+|r_1^-|^2+2(\mu a_{\mathrm{CT}} a_{\mathrm{CT}})^2 - 2a_{\mathrm{CT}} a_{\mathrm{TR}} \mu \Re\left\{r_0^+ \mathsf{e}^{\mathsf{j}\theta_a}\right\} - 2a_{\mathrm{CT}} a_{\mathrm{CT}} \mu \Re\left\{r_0^- \mathsf{e}^{\mathsf{j}\theta_b}\right\}\right)}. \tag{4.6}$$

In order to eliminate the random phases $\theta_a$ and $\theta_b$, we make use of the following identity [30] (pp. 449)

$$\frac{1}{2\pi} \int_0^{2\pi} \mathsf{e}^{c(a\cos(\phi) \pm b\sin(\phi))} \mathsf{d}\phi = \mathsf{I}_0\left(c\sqrt{a^2+b^2}\right). \tag{4.7}$$

If we take expected value with respect to $\theta_a$ and $\theta_b$ in (4.6) and we use Eq. (4.7) we obtain

$$\begin{aligned} &f_{\mathbf{r}|H_0,a_{\mathrm{CT}},a_{\mathrm{CT}}}(\mathbf{r}|H_0, a_{\mathrm{CT}}, a_{\mathrm{TR}}) = \mathop{\mathbb{E}}_{\theta_a,\theta_b}\left[f_{\mathbf{r}|H_0,a_{\mathrm{CT}},a_{\mathrm{TR}},\theta_a,\theta_b}(\mathbf{r}|H_0, a_{\mathrm{CT}}, a_{\mathrm{TR}}, \theta_a, \theta_b)\right] \overset{(4.7)}{=} \\ &= \frac{1}{\left(\pi\sigma_A^2\right)^4} \mathsf{e}^{-\frac{1}{\sigma_A^2}\left(|r_0^+|^2+|r_0^-|^2+|r_1^+|^2+|r_1^-|^2+2(\mu a_{\mathrm{CT}} a_{\mathrm{CT}})^2\right)} \mathsf{I}_0\left(\frac{2\mu a_{\mathrm{CT}} a_{\mathrm{TR}} |r_0^+|}{\sigma_A^2}\right) \mathsf{I}_0\left(\frac{2\mu a_{\mathrm{CT}} a_{\mathrm{TR}} |r_0^-|}{\sigma_A^2}\right). \end{aligned} \tag{4.8}$$

[3]Note that $f_{\mathbf{r}|H_0}(\cdot|\cdot)$ is identical with $f_{\mathbf{r}|\mathbf{s}_0}(\cdot|\cdot)$.

If we use expectation with respect to $a_{\mathrm{CT}}$ and $a_{\mathrm{TR}}$ in Eq.(4.8) we obtain the desired conditional pdf. However, the integral

$$\int_0^{+\infty}\int_0^{+\infty} f_{\mathbf{r}|H_0,a_{\mathrm{CT}},a_{\mathrm{CT}}}(\mathbf{r}|H_0,x,y)f_{a_{\mathrm{CT}}}(x)f_{a_{\mathrm{TR}}}(y)\mathsf{d}x\mathsf{d}y$$

does not admit closed form (for any value of $K_l \in [0,\infty), l \in \{\mathrm{CT},\mathrm{TR}\}$ in Eq. (4.1)) and thus the conditional pdf $f_{\mathbf{r}|H_0}(\mathbf{r}|H_0)$ cannot be given in closed form. In a straightforward manner, it can be shown that neither $f_{\mathbf{r}|H_1}(\mathbf{r}|H_1)$ has closed form (due to symmetry of the problem) and thus ML noncoherent symbol-by-symbol detection cannot be derived for backscatter FSK.

**ML detection for $K_{\mathrm{CT}} = K_{\mathrm{TR}} = \infty$**

For the special case where Rician $K_l$ factor is equal to infinity for each link, i.e. $K_{\mathrm{CT}} = K_{\mathrm{TR}} = \infty$, there is no fading, and thus, fading parameters are equal to unity (i.e. $a_{\mathrm{CT}} = a_{\mathrm{TR}} = 1$) and $\phi_{\mathrm{CT}}, \phi_{\mathrm{TR}} \sim \mathcal{U}[0, 2\pi)$. In such case, the joint pdf of random vector $\mathbf{r}$ given $H_0$ and all parameters factorizes as

$$\begin{aligned} &f_{\mathbf{r}|H_0,a_{\mathrm{CT}},a_{\mathrm{TR}},\theta_a,\theta_b}(\mathbf{r}|H_0,a_{\mathrm{CT}},a_{\mathrm{TR}},\theta_a,\theta_b) = f_{\mathbf{r}|H_0,\theta_a,\theta_b}(\mathbf{r}|H_0,\theta_a,\theta_b) \\ &= f_{r_0^+|H_0,\theta_a}(r_0^+|H_0,\theta_a)f_{r_0^-|H_0,\theta_b}(r_0^-|H_0,\theta_b)f_{r_1^+|H_0}(r_1^+|H_0)f_{r_1^-|H_0}(r_1^-|H_0). \end{aligned}$$

If we utilize Eq. (4.8) we obtain the conditional pdf $f_{\mathbf{r}|H_0}(\mathbf{r}|H_0)$ as

$$\begin{aligned} f_{\mathbf{r}|H_0}(\mathbf{r}|H_0) &= \mathop{\mathbb{E}}_{\theta_a,\theta_b}\left[f_{\mathbf{r}|H_0,\theta_a,\theta_b}(\mathbf{r}|H_0,\theta_a,\theta_b)\right] \overset{(4.8)}{=} \\ &= \frac{1}{\left(\pi\sigma_A^2\right)^4}\mathsf{e}^{-\frac{1}{\sigma_A^2}\left(|r_0^+|^2+|r_0^-|^2+|r_1^+|^2+|r_1^-|^2+2(\mu)^2\right)}\mathsf{I}_0\!\left(\frac{2\mu|r_0^+|}{\sigma_A^2}\right)\mathsf{I}_0\!\left(\frac{2\mu|r_0^-|}{\sigma_A^2}\right). \end{aligned} \tag{4.9}$$

Similarly, if we follow the same procedure for hypothesis $H_1$ we obtain that

$$f_{\mathbf{r}|H_1}(\mathbf{r}|H_1) = \frac{1}{\left(\pi\sigma_A^2\right)^4}\mathsf{e}^{-\frac{1}{\sigma_A^2}\left(|r_0^+|^2+|r_0^-|^2+|r_1^+|^2+|r_1^-|^2+2(\mu)^2\right)}\mathsf{I}_0\!\left(\frac{2\mu|r_1^+|}{\sigma_A^2}\right)\mathsf{I}_0\!\left(\frac{2\mu|r_1^-|}{\sigma_A^2}\right). \tag{4.10}$$

Consequently, the ML detection rule of Eq. (4.3) for the special case of no fading can be written as

$$\mathsf{I}_0\!\left(\frac{2\mu|r_0^+|}{\sigma_A^2}\right)\mathsf{I}_0\!\left(\frac{2\mu|r_0^-|}{\sigma_A^2}\right) \underset{H_1}{\overset{H_0}{\gtrless}} \mathsf{I}_0\!\left(\frac{2\mu|r_1^+|}{\sigma_A^2}\right)\mathsf{I}_0\!\left(\frac{2\mu|r_1^-|}{\sigma_A^2}\right). \tag{4.11}$$

If we use the definition of average received SNR of Eq.(2.27) we can express the detection rule as a function of observations. Firstly, we note that

$$\mathtt{SNR} = \frac{8s^2 P_C}{\pi^2 \sigma_n^2} L = \frac{\tilde{m}_1^2 L^2}{4a^2 \sigma_n^2 L} = \frac{2\mu^2}{\sigma_A^2} \implies \frac{\mu}{\sigma_A} = \frac{\mathtt{SNR}}{\sqrt{2}}. \tag{4.12}$$

Thus the ML detector for noncoherent backscatter FSK can be expressed as follows

$$\mathsf{I}_0\left(\frac{\sqrt{2\mathtt{SNR}}}{\sigma_A}|r_0^+|\right)\mathsf{I}_0\left(\frac{\sqrt{2\mathtt{SNR}}}{\sigma_A}|r_0^-|\right) \underset{H_1}{\overset{H_0}{\gtrless}} \mathsf{I}_0\left(\frac{\sqrt{2\mathtt{SNR}}}{\sigma_A}|r_1^+|\right)\mathsf{I}_0\left(\frac{\sqrt{2\mathtt{SNR}}}{\sigma_A}|r_1^-|\right). \tag{4.13}$$

It is noted that the above detector requires the knowledge of the average received SNR, as well as the variance of noise $\sigma_A^2$ for the detection rule, which may be impractical in many scenarios. As an alternative, the following detection rule may be utilized

$$\mathsf{I}_0\Big(\sqrt{2}|r_0^+|\Big)\mathsf{I}_0\Big(\sqrt{2}|r_0^-|\Big) \underset{H_1}{\overset{H_0}{\gtrless}} \mathsf{I}_0\Big(\sqrt{2}|r_1^+|\Big)\mathsf{I}_0\Big(\sqrt{2}|r_1^-|\Big). \tag{4.14}$$

Simulation results show the knowledge of average received SNR and noise variance ($\sigma_A^2$) of the ML detector (Eq. (4.13)) offers negligible BER performance gains over the detector of Eq. (4.14).

### Composite Hypothesis Testing Noncoherent FSK Detection

Firstly, we define $h \triangleq \frac{\tilde{m}_1 L}{2}\mathsf{e}^{-\mathrm{j}\phi_1} \in \mathbb{C}$, which stands for the compound channel hyperparameter. Then the baseband equivalent signal for a single bit duration of Eq. (2.17) can rewritten as:

$$\mathbf{r} = h\mathbf{s}_i \odot \begin{bmatrix} \mathsf{e}^{+\mathrm{j}\Phi_0} \\ \mathsf{e}^{-\mathrm{j}\Phi_0} \\ \mathsf{e}^{+\mathrm{j}\Phi_1} \\ \mathsf{e}^{-\mathrm{j}\Phi_1} \end{bmatrix} + \mathbf{n}, \quad i \in \mathbb{B}. \tag{4.15}$$

This work proposes a composite hypothesis testing detection rule which is given by

$$\mathop{\mathbb{E}}_{\Phi_0}\left[\max_{h\in\mathbb{C}} \ln\left(f_{\mathbf{r}|\mathbf{s}_0,h,\Phi_0}(\mathbf{r}|\mathbf{s}_0,h,\Phi_0)\right)\right] \underset{H_1}{\overset{H_0}{\gtrless}} \mathop{\mathbb{E}}_{\Phi_1}\left[\max_{h\in\mathbb{C}} \ln\left(f_{\mathbf{r}|\mathbf{s}_1,h,\Phi_1}(\mathbf{r}|\mathbf{s}_1,h,\Phi_1)\right)\right]. \tag{4.16}$$

**Proposition 4.1.** *The detector of Eq,* (4.16) *can be expressed equivalently, as:*

$$z_0 \triangleq |r_0^+|^2 + |r_0^-|^2 \underset{H_1}{\overset{H_0}{\gtrless}} |r_1^+|^2 + |r_1^-|^2 \triangleq z_1. \tag{4.17}$$

*Proof.* In order to calculate the inner maximizations of Eq. (4.16) we set

$$\mathbf{t}_i(\Phi_i) = \left[\mathsf{e}^{+\mathrm{j}\Phi_0}, \mathsf{e}^{-\mathrm{j}\Phi_0}, \mathsf{e}^{+\mathrm{j}\Phi_1}, \mathsf{e}^{-\mathrm{j}\Phi_1}\right]^\top \odot \mathbf{s}_i, \quad i \in \mathbb{B}.$$

It can be easily shown from Eqs. (4.15) and (2.18) that

$$f_{\mathbf{r}|\mathbf{s}_i,h,\Phi_i}(\mathbf{r}|\mathbf{s}_i,h,\Phi_i) \sim \mathcal{CN}\left(h\mathbf{t}_i(\Phi_i), 2\sigma^2\mathbf{I}_4\right), \quad i \in \mathbb{B},$$

where for simplicity we set $\sigma^2 = \sigma_n^2 L$. The quantity of the left-hand side (LHS) of Eq. (4.16) is firstly calculated as

$$\begin{aligned}\arg\max_{h\in\mathbb{C}} \ln\left(f_{\mathbf{r}|\mathbf{s}_0,h,\Phi_0}(\mathbf{r}|\mathbf{s}_0,h,\Phi_0)\right) &= \arg\max_{h\in\mathbb{C}} -\frac{1}{2\sigma^2}\left|\left|\mathbf{r} - h\mathbf{t}_0(\Phi_0)\right|\right|_2^2 \\ &= \arg\min_{h\in\mathbb{C}} \left|\left|\mathbf{r} - h\mathbf{t}_0(\Phi_0)\right|\right|_2^2 \Longrightarrow h_{\text{opt}} = \frac{\left(\mathbf{t}_0(\Phi_0)\right)^{\mathrm{H}}\mathbf{r}}{\left|\left|\mathbf{t}_0(\Phi_0)\right|\right|_2^2}.\end{aligned}$$

Hence,

$$\begin{aligned}&\max_{h\in\mathbb{C}} \ln\left(f_{\mathbf{r}|\mathbf{s}_0,h,\Phi_0}(\mathbf{r}|\mathbf{s}_0,h,\Phi_0)\right) = \ln\left(f_{\mathbf{r}|\mathbf{s}_0,h,\Phi_0}(\mathbf{r}|\mathbf{s}_0,h_{\text{opt}},\Phi_0)\right) \\ &= \ln\left(\left(\frac{1}{\pi\left(2\sigma^2\right)}\right)^4\right) - \frac{1}{2\sigma^2}\left(\left|\left|\mathbf{r} - \frac{\left(\mathbf{t}_0(\Phi_0)\right)^{\mathrm{H}}\mathbf{r}}{\left|\left|\mathbf{t}_0(\Phi_0)\right|\right|_2^2}\mathbf{t}_0(\Phi_0)\right|\right|_2^2\right) \\ &= 4\ln\left(\frac{1}{2\pi\sigma^2}\right) - \frac{1}{2\sigma^2}\left(\left|\left|\mathbf{r}\right|\right|_2^2 - \frac{|\mathbf{r}^{\mathrm{H}}\mathbf{t}_0(\Phi_0)|^2}{\left|\left|\mathbf{t}_0(\Phi_0)\right|\right|_2^2}\right) \\ &= 4\ln\left(\frac{1}{2\pi\sigma^2}\right) - \frac{1}{4\sigma^2}\left(2\left|\left|\mathbf{r}\right|\right|_2^2 - \left|(r_0^+)^*\mathsf{e}^{\mathrm{j}\Phi_0} + (r_0^-)^*\mathsf{e}^{-\mathrm{j}\Phi_0}\right|^2\right) \\ &= 4\ln\left(\frac{1}{2\pi\sigma^2}\right) - \frac{1}{2\sigma^2}\left|\left|\mathbf{r}\right|\right|_2^2 + \frac{1}{4\sigma^2}\left(|r_0^+|^2 + |r_0^-|^2\right) + \frac{1}{2\sigma^2}\Re\left\{(r_0^+)^*(r_0^-)\mathsf{e}^{2\mathrm{j}\Phi_0}\right\}.\end{aligned} \tag{4.18}$$

Only the last term in Eq. (4.18) depends on $\Phi_0$. Thus, expectation with respect to $\Phi_0$ in the last term of Eq.(4.18) offers

$$\mathop{\mathbb{E}}_{\Phi_0}\left[\Re\left\{(r_0^+)^*(r_0^-)\mathsf{e}^{2\mathrm{j}\Phi_0}\right\}\right] = \mathop{\mathbb{E}}_{\Phi_0}\left[\Re\left\{(r_0^+)^*(r_0^-)\right\}\cos(2\Phi_0)\right] - \mathop{\mathbb{E}}_{\Phi_0}\left[\Im\left\{(r_0^+)^*(r_0^-)\right\}\sin(2\Phi_0)\right] = 0.$$

Therefore, if we take expectation with respect to $\Phi_0$ in Eq. (4.18) the last term vanishes and the LHS of Eq. (4.16) can be written as

$$\mathop{\mathbb{E}}_{\Phi_0}\left[\max_{h\in\mathbb{C}} \ln\left(f_{\mathbf{r}|\mathbf{s}_0,h,\Phi_0}(\mathbf{r}|\mathbf{s}_0,h,\Phi_0)\right)\right] = 4\ln\left(\frac{1}{2\pi\sigma^2}\right) - \frac{1}{2\sigma^2}||\mathbf{r}||_2^2 + \frac{1}{4\sigma^2}\left(|r_0^+|^2+|r_0^-|^2\right). \quad (4.19)$$

The same reasoning can be easily applied to the right-hand side (RHS) of Eq. (4.16), which can be expressed as

$$\mathop{\mathbb{E}}_{\Phi_1}\left[\max_{h\in\mathbb{C}} \ln\left(f_{\mathbf{r}|\mathbf{s}_1,h,\Phi_1}(\mathbf{r}|\mathbf{s}_1,h,\Phi_1)\right)\right] = 4\ln\left(\frac{1}{2\pi\sigma^2}\right) - \frac{1}{2\sigma^2}||\mathbf{r}||_2^2 + \frac{1}{4\sigma^2}\left(|r_1^+|^2+|r_1^-|^2\right). \quad (4.20)$$

Thus after elementary calculations the detection rule of Eq. (4.17) is obtained. □

The above detector is also known as square-law detector and has also been proposed by [13] as a heuristic noncoherent detection rule. In contrary, this work shows that the above rule is a result of a composite hypothesis testing problem. It is noted that the above rule does not require the channel statistics and is solely based on the received information. The above detection test is applied to each symbol of the received sequence.

**BER Analysis of Composite Hypothesis Testing Detector for Rayleigh Fading ($K_{\mathrm{CT}} = K_{\mathrm{TR}} = 0$)**

Under hypothesis $H_0$ and given all the random parameters $\{a_{\mathrm{CT}}, a_{\mathrm{TR}}, \phi_1, \Phi_0, \Phi_1\}$, the output has the following statistics

$$r_0^+ \sim \mathcal{CN}\left(\frac{\tilde{m}_1 L}{2}\mathrm{e}^{\mathrm{j}(-\phi_1+\Phi_0)}, 2\sigma_n^2 L\right), \quad r_1^+ \sim \mathcal{CN}\left(0, 2\sigma_n^2 L\right),$$
$$r_0^- \sim \mathcal{CN}\left(\frac{\tilde{m}_1 L}{2}\mathrm{e}^{\mathrm{j}(-\phi_1-\Phi_0)}, 2\sigma_n^2 L\right), \quad r_1^- \sim \mathcal{CN}\left(0, 2\sigma_n^2 L\right).$$

Random variable $z_1$ is the sum of 4 independent squared zero-mean Gaussian r.v.'s with variance $\sigma \triangleq \sigma_n L$, thus under $H_0$ r.v. $z_1$ follows a Chi-squared distribution with 4 degrees of freedom [23]

$$f_{z_1|H_0}(z_1|H_0) = \frac{z_1}{4\sigma^4}\mathrm{e}^{-\frac{z_1}{2\sigma^2}}, \quad z_1 \geq 0. \quad (4.21)$$

Random variable $z_0$ is the sum of 4 independent squared non-zero-mean Gaussian r.v.'s, each of variance $\sigma^2$, and thus, it follows noncentral Chi-squared with 4 degrees of freedom

with noncentrality parameter [23]

$$s^2 = \left|\frac{\tilde{m}_1 L}{2}\mathsf{e}^{\mathsf{j}(-\phi_1+\Phi_0)}\right|^2 + \left|\frac{\tilde{m}_1 L}{2}\mathsf{e}^{\mathsf{j}(-\phi_1-\Phi_0)}\right|^2 = \frac{(\tilde{m}_1 L)^2}{2}.$$

If we abbreviate

$$a \triangleq a_{\mathrm{CT}} a_{\mathrm{TR}}$$
$$\mu \triangleq \frac{\tilde{m}_1 L}{2a}$$

(hence $s^2 = 2(\mu a)^2$), then the conditional pdf of r.v. $z_0$ given hypothesis $H_0$ and the random amplitude $a$ is expressed as [23][4]

$$f_{z_0|H_0,a}(z_0|H_0,a) = \frac{\sqrt{z_0}}{2\sigma^2\sqrt{2}(\mu a)}\mathsf{e}^{-\frac{z_0+2(\mu a)^2}{2\sigma^2}}\mathsf{I}_1\left(\frac{\sqrt{2z_0}(\mu a)}{\sigma^2}\right), \quad z_0 \geq 0. \tag{4.22}$$

Note that in backscatter FSK the average received SNR is

$$\mathtt{SNR} = \frac{8s^2 P_C}{\pi^2\sigma_n^2}L = \frac{\tilde{m}_1^2 L^2}{4a^2\sigma_n^2 L} = \frac{\mu^2}{\sigma^2} \implies \frac{\mu}{\sigma} = \sqrt{\mathtt{SNR}}. \tag{4.23}$$

The probability of error of the detector of Eq. (4.17) can be offered in closed form for the special case of Rician parameters $K_{\mathrm{CT}} = K_{\mathrm{TR}} = 0$. In such case, the pdf of r.v.'s $a_{\mathrm{CT}}$ and $a_{\mathrm{TR}}$ is expressed as

$$f_{a_l}(x) = 2\ x\ \mathsf{e}^{-x^2},\ x \geq 0, \quad l \in \{\mathrm{CT}, \mathrm{TR}\}.$$

Hence, the joint pdf of r.v. $a = a_{\mathrm{CT}} a_{\mathrm{TR}}$ is given by Eq. (2.29).

It can be shown that $f_{z_0|H_0}(z_0|H_0) = \mathop{\mathbb{E}}_{a}\left[f_{z_0|H_0,a}(z_0|H_0,a)\right]$ does not admit closed form expression. However, if we define the random variable $z \triangleq \frac{z_0}{z_1}$, it turns out that the pdf of $z$ given $H_0$ can be found in closed form which will help us to find in closed form the probability of bit error. The pdf of r.v. $z$ given $H_0$ and $a$ is expressed as [25] (pp. 276)

$$f_{z|H_0,a}(z|H_0,a) = \int_0^{+\infty} y f_{z_0|H_0,a}(yz|H_0,a) f_{z_1|H_0}(y|H_0)\mathsf{d}y, \tag{4.24}$$

[4]It noted that $f_{z_0|H_0,a_{\mathrm{CT}},a_{\mathrm{TR}},\Phi_0}(z_0|H_0,a_{\mathrm{CT}},a_{\mathrm{TR}},\Phi_0) = f_{z_0|H_0,a}(z_0|H_0,a)$.

thus if we substitute Eqs. (4.21) and (4.22) in Eq.(4.24) we obtain

$$f_{z|H_0,a}(z|H_0,a) = \int_0^{+\infty} y \frac{\sqrt{zy}}{2\sigma^2\sqrt{2}(\mu a)} \mathsf{e}^{-\frac{zy+2(\mu a)^2}{2\sigma^2}} \mathsf{I}_1\left(\frac{\sqrt{2zy}(\mu a)}{\sigma^2}\right) \frac{y}{4\sigma^4} \mathsf{e}^{-\frac{y}{2\sigma^2}} \mathsf{d}y$$
$$= \frac{\mathsf{e}^{-\frac{(a\mu)^2}{\sigma^2(1+z)}} z\Big((a\mu)^4 z^2 + 6(a\mu)^2\sigma^2 z(1+z) + 6\sigma^4(1+z)^2\Big)}{\sigma^4(1+z)^6}, \tag{4.25}$$

where we used Eq. (6.643.2) from [26] to obtain Eq.(4.25). If we substitute Eq. (4.23) in Eq. (4.25) we obtain that

$$f_{z|H_0,a}(z|H_0,a) = \frac{\mathsf{e}^{-\frac{a^2\mathtt{SNR}}{(1+z)}} z\Big(a^4\mathtt{SNR}^2 z^2 + 6a^2\mathtt{SNR} z(1+z) + 6(1+z)^2\Big)}{(1+z)^6}. \tag{4.26}$$

Now, we can calculate the conditional pdf of r.v. $z$ given hypothesis $H_0$ as follows

$$f_{z|H_0}(z|H_0) = \mathop{\mathbb{E}}_{a}\left[f_{z|H_0,a}(z|H_0,a)\right]$$
$$= \int_0^{+\infty} \frac{\mathsf{e}^{-\frac{a^2\mathtt{SNR}}{(1+z)}} z\Big(a^4\mathtt{SNR}^2 z^2 + 6a^2\mathtt{SNR} z(1+z) + 6(1+z)^2\Big)}{(1+z)^6}\, 4a\mathsf{K}_0(2a)\, \mathsf{d}a$$
$$= \frac{z\mathsf{e}^{\frac{1+z}{\mathtt{SNR}}}\big(z^2(1+z)^2 + 2\mathtt{SNR}^2(3+3z+z^2) + 2\mathtt{SNR}(3+5z+2z^2)\big)\Gamma\big(0, \frac{1+z}{\mathtt{SNR}}\big)}{\mathtt{SNR}^3(1+z)^3}$$
$$- \frac{\mathtt{SNR} z^2\big(z(1+z) + \mathtt{SNR}(2+z)\big)}{\mathtt{SNR}^3(1+z)^3}, \tag{4.27}$$

where in order to derive Eq.(4.27) we used Eq. (6.631.3) from [26]. $\Gamma(s,x)$ is the "upper" incomplete Gamma function and its definition can be found in Appendix (Eq. (A.4)).

The square-law detector for bistatic scatter radio FSK can be written in compact form as

$$z_0 \underset{H_1}{\overset{H_0}{\gtrless}} z_1 \Longleftrightarrow z \underset{H_1}{\overset{H_0}{\gtrless}} 1. \tag{4.28}$$

Given hypothesis $H_0$, an error occurs if r.v. $z$ is less than 1; the probability of such event

is given by

$$\begin{aligned}\Pr(e|H_0) = \Pr(z<1|H_0) &= \int_0^1 f_{z|H_0}(z|H_0) \\ &= -\frac{\mathtt{SNR}+\mathsf{e}^{\frac{2}{\mathtt{SNR}}}\big(5\mathtt{SNR}+2\big)\mathsf{Ei}\big(-\frac{2}{\mathtt{SNR}}\big)}{4\mathtt{SNR}^2},\end{aligned} \tag{4.29}$$

where we used Eq. (6.455.1) from [26] to derive the above equation. The definition of function $\mathsf{Ei}(x)$ can be found in Appendix Eq (A.3). Due to the symmetry of the problem it can be easily proved that $\Pr(e|H_0) = \Pr(e|H_1)$ and thus, $\Pr(e) = \Pr(e|H_0)$.

### 4.1.2 Noncoherent Decoding

The tag encodes a sequence of $dK$ information bits into a sequence of $dN$ coded bits for some $d \in \mathbb{N}$, where $dN$ is the size of the packet. $N$ stands for the codeword length, hence, $d$ can be considered as the depth of the interleaver, which may be utilized in conjunction with coding process.

Let channel coherence time be smaller than the duration of $d$ codebits. Then the received de-interleaved symbols corresponding to a codeword undergo independent fading. Let $\mathbf{c} = [c_1, c_2, \ldots, c_N] \in \mathcal{C}$ be a codeword corresponding to a specific row of interleaving matrix; then according to Eq.(4.15) the discrete baseband equivalent for a sequence of $N$ de-interleaved symbols of a single row is given by

$$\mathbf{r}_{1:N} = \begin{bmatrix} \mathbf{r}_1 \\ \mathbf{r}_2 \\ \vdots \\ \mathbf{r}_N \end{bmatrix} = \begin{bmatrix} h_1\mathbf{t}_{c_1}(\Phi_{c_1}) \\ h_2\mathbf{t}_{c_2}(\Phi_{c_2}) \\ \vdots \\ h_N\mathbf{t}_{c_N}(\Phi_{c_N}) \end{bmatrix} + \begin{bmatrix} \mathbf{n}_1 \\ \mathbf{n}_2 \\ \vdots \\ \mathbf{n}_N \end{bmatrix}, \tag{4.30}$$

where, we set $\mathbf{r}_n = \big[r_0^+(n), r_0^-(n), r_1^+(n), r_1^-(n)\big]^\top$ and $\mathbf{t}_{c_n}(\Phi_{c_n}) = \big[\mathsf{e}^{+\mathsf{j}\Phi_0}, \mathsf{e}^{-\mathsf{j}\Phi_0}, \mathsf{e}^{+\mathsf{j}\Phi_1}, \mathsf{e}^{-\mathsf{j}\Phi_1}\big]^\top \odot \mathbf{s}_{c_n}$, with $\mathbf{s}_{c_n} = [1-c_n, 1-c_n, c_n, c_n]^\top$, $c_n \in \mathbb{B}$, $n = 1, ..., N$. The parameters $h_1, h_2, \ldots, h_N$ are independent random channel coefficients due to independent fading. The noise statistics for the sequence of the $N$ symbols are $[\mathbf{n}_1, \mathbf{n}_2, \ldots, \mathbf{n}_N]^\top \sim \mathcal{CN}\left(\mathbf{0}_{4N}, 2\sigma^2\mathbf{I}_{4N}\right)$, where $\sigma^2$ is defined as in previous subsection. As in the uncoded case, the ML decoding rule cannot be given in closed form, hence, an alternative decoding technique should be utilized.

In this work, we make use of the following decoding rule

$$\widehat{\mathbf{c}} = \arg\max_{\mathbf{c}\in\mathcal{C}} \mathop{\mathbb{E}}_{\Phi_0,\Phi_1}\left[\max_{\mathbf{h}\in\mathbb{C}^N} \mathsf{ln}\big(f_{\mathbf{r}_{1:N}|\mathbf{c},\mathbf{h},\Phi_0,\Phi_1}(\mathbf{r}_{1:N}|\mathbf{c},\mathbf{h},\Phi_0,\Phi_1)\big)\right], \tag{4.31}$$

where we abbreviated $\mathbf{h} = [h_1, h_2, \ldots, h_N]^\top$.

**Theorem 4.2.** *If $dT \geq T_{\text{coh}}$, then the decoding rule of Eq. (4.31) is simplified to the following decoding rule*

$$\widehat{\mathbf{c}} = \arg\max_{\mathbf{c}\in\mathcal{C}} \mathbf{w}\mathbf{c}^\top, \tag{4.32}$$

*where $\mathbf{w} = [w(1), w(2), \ldots, w(N)] \triangleq \{z_1(n) - z_0(n)\}_{n=1}^N$, a $N-$dimensional real row vector with $z_i(n) \triangleq |r_i^+(n)|^2 + |r_i^-(n)|^2, i \in \mathbb{B}$.*

*Proof.* If we exploit the conditional independence of each $\mathbf{r}_n$ given the transmitted codeword $\mathbf{c}$ and given the parameters $\mathbf{h}, \Phi_0, \Phi_1$, the inner maximization of Eq. (4.31) can be expressed as the sum of independent maximization, i.e.,

$$\max_{\mathbf{h}\in\mathbb{C}^N} \mathsf{ln}\big(f_{\mathbf{r}_{1:N}|\mathbf{c},\mathbf{h},\Phi_0,\Phi_1}(\mathbf{r}_{1:N}|\mathbf{c},\mathbf{h},\Phi_0,\Phi_1)\big) = \sum_{n=1}^N \max_{h_n\in\mathbb{C}} \mathsf{ln}\big(f_{\mathbf{r}_n|c_n,h_n,\Phi_{c_n}}(\mathbf{r}_n|c_n,h_n,\Phi_{c_n})\big)\,. \tag{4.33}$$

Eq. (4.18) reveals the way to calculate the value for each individual maximization within the summation. Due to the linearity of expectation operation, if we take expectations with respect to $\Phi_0$ and $\Phi_1$ in Eq. (4.33) we obtain

$$\begin{aligned}\mathop{\mathbb{E}}_{\Phi_0,\Phi_1}\left[\sum_{n=1}^N Q_n + A_{c_n}\right] &= \sum_{n=1}^N \mathop{\mathbb{E}}_{\Phi_0,\Phi_1}[Q_n + A_{c_n}] = \sum_{n=1}^N Q_n + (1-c_n)\mathop{\mathbb{E}}_{\Phi_0}[A_0] + c_n \mathop{\mathbb{E}}_{\Phi_1}[A_1] \\ &= \sum_{n=1}^N Q_n + \mathop{\mathbb{E}}_{\Phi_0}[A_0] + c_n\left(\mathop{\mathbb{E}}_{\Phi_1}[A_1] - \mathop{\mathbb{E}}_{\Phi_0}[A_0]\right), \end{aligned} \tag{4.34}$$

where,

$$A_{c_n} \triangleq \frac{1}{4\sigma^2}\left(|r_{c_n}^+(n)|^2 + |r_{c_n}^-(n)|^2\right) + \frac{1}{2\sigma^2}\Re\left\{(r_{c_n}^+(n))^*(r_{c_n}^-(n))\mathsf{e}^{2\mathsf{j}\Phi_{c_n}}\right\}. \tag{4.35}$$

$$Q_n \triangleq 4\mathsf{ln}\left(\frac{1}{2\pi\sigma^2}\right) - \frac{1}{2\sigma^2}||\mathbf{r}_n||_2^2. \tag{4.36}$$

As in the uncoded case, the second terms of $A_0$ and $A_1$ vanish by taking expectations, and

thus, the outer maximization of Eq. (4.31) can be expressed as follows

$$\begin{aligned}
\widehat{\mathbf{c}} &= \arg\max_{\mathbf{c}\in\mathcal{C}} \left\{ \sum_{n=1}^{N} Q_n + \mathop{\mathbb{E}}_{\Phi_0}[A_0] + c_n \left( \mathop{\mathbb{E}}_{\Phi_1}[A_1] - \mathop{\mathbb{E}}_{\Phi_0}[A_0] \right) \right\} \\
&= \arg\max_{\mathbf{c}\in\mathcal{C}} \sum_{n=1}^{N} c_n \left( \mathop{\mathbb{E}}_{\Phi_1}[A_1] - \mathop{\mathbb{E}}_{\Phi_0}[A_0] \right) \\
&= \arg\max_{\mathbf{c}\in\mathcal{C}} \sum_{n=1}^{N} c_n \left( \, |r_1^+(n)|^2 + |r_1^-(n)|^2 - \left( |r_0^+(n)|^2 + |r_0^-(n)|^2 \right) \right) \\
&= \arg\max_{\mathbf{c}\in\mathcal{C}} \mathbf{w}\mathbf{c}^\top.
\end{aligned}$$

□

The corresponding information bit sequence $\widehat{\mathbf{b}}$ can be then extracted from $\widehat{\mathbf{c}}$. Therefore, the receiver constructs the row vector $\mathbf{w}$ for each $N$ symbols and applies the rule of Eq. (4.32) $d$ times. Clearly the above derivation applies only when $dT \geq T_{\text{coh}}$, however, in this work the rule of Eq. (4.32) is utilized for any value of $d$ (even when $dT < T_{\text{coh}}$), due to its inherent simplicity. Apparently, if $dT < T_{\text{coh}}$, then, the rule of Eq. (4.32) is suboptimal.

The optimization problem of Eq. (4.32) has exponential complexity on the dimension of the code $K$ (due to the exhaustive search on all possible $N$–tuples of set $\mathcal{C}$). However, if small length $N$ (and thus small $K$) is utilized, then Eq. (4.32) can be computed with low computational complexity cost. For simulation results, small block length Reed-Muller as well as BCH channel codes are studied with good error correction capabilities [29, 31].

Fig. 4.1 depicts the whole signal processing chain of noncoherent FSK with channel coding in bistatic backscatter radio. It is noted that the output of demodulator produces 4 complex numbers (i.e. $r_0^+, r_0^-, r_1^+, r_1^-$) corresponding to a single transmitted bit, hence for a block of $N_{\text{TOT}} = dN$ transmitted bits the output produces $N_{\text{TOT}}$ symbols ($4N_{\text{TOT}}$ complex numbers). The block SLSIC (square-law soft information combiner) converts every sequence of $N$ symbols in the rows of interleaving matrix to the corresponding soft information vector $\mathbf{w}$.

### 4.1.3 Simulation Results

The first set of simulations is conducted for bistatic scatter radio system of Fig. 2.1 with uncoded as well as coded noncoherent FSK assuming that each link suffers from Rayleigh

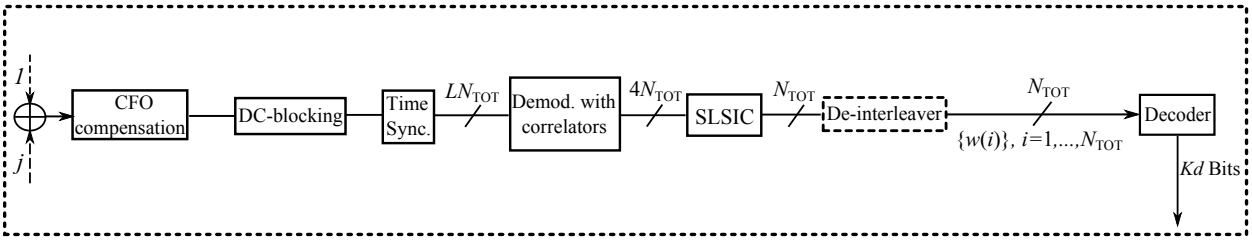


Figure 4.1: Complete signal processing chain with channel coding for noncoherent FSK in bistatic backscatter radio.

fading (i.e. $K_{\mathrm{CT}} = K_{\mathrm{TR}} = 0$).[5] The impact of carrier emitter-SDR reader link on the overall BER performance is also discussed. Afterwards, the same simulation study is carried out for Rician fading. In all simulation results the parameters `CSR` and oversampling factor $L$, are set 20dB and 100 samples per bit, respectively. The impact of several communication parameters in BER performance is presented for both fading scenarios.

In the coded setups is assumed that the system operates in the power limited regime. More specifically, if the transmitter wants to send a packet of $K$ information bits and has energy budget $E$ Joules per transmitted packet, it utilizes $E_b = \frac{E}{K}$ Joules per bit. If the transmitter sends $N \geq K$ coded bits within the packet, it spends energy $E_b \frac{K}{N}$ Joules per coded bit which is less or equal to $E_b$. In other words, the total energy budget per packet transmission is the same, either when coding is employed ($N$ transmitted bits), or when no coding is employed ($K \leq N$ transmitted bits).

### Rayleigh Fading ($K_{\mathrm{CT}} = K_{\mathrm{TR}} = 0$)

Regarding the uncoded setup, the coherence time $T_{\mathrm{coh}}$ was assumed to span 100 bit periods. Fig. 4.2 depicts the simulated, as well as the analytical BER performance of the detector of Eq. (4.17) as a function of average received SNR, `SNR`, given by Eq. (2.27). We note that the analytical BER performance of Eq. (4.29) perfectly matches with simulation results.

For the coded setup, noncoherent FSK with Reed Muller (RM) channel code $\mathcal{C}_{\mathrm{RM}}$ and parameters $(32, 16, 8)$ is considered.[6] Firstly, the impact of deep fading is illustrated when codes of small block length are utilized. In the scenario of Fig. 4.3 we fix the value of $T_{\mathrm{coh}} = 100T$ and we examine the impact of the interleaving depth. It is observed that as

[5]The uncoded scheme in the figures of Rayleigh fading scenario correspond to the square-law detector (Eq. (4.17)).

[6]The specific code has the best coding gain over all Reed-Muller codes up to length $N = 32$ (Table I columns 2-3 in [32]).

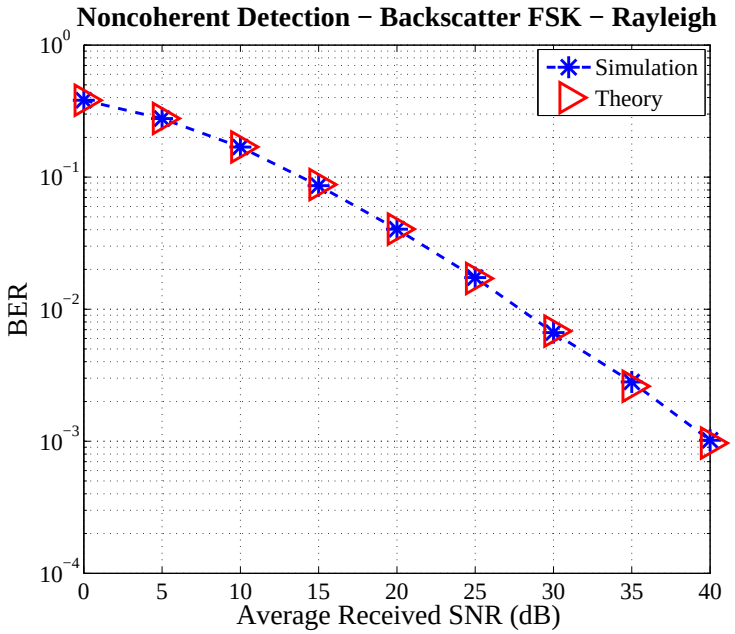


Figure 4.2: BER performance as a function of SNR for uncoded noncoherent bistatic scatter radio FSK (with $K_{\mathrm{CT}} = K_{\mathrm{TR}} = 0$). It is noted that simulation results perfectly match with analysis.

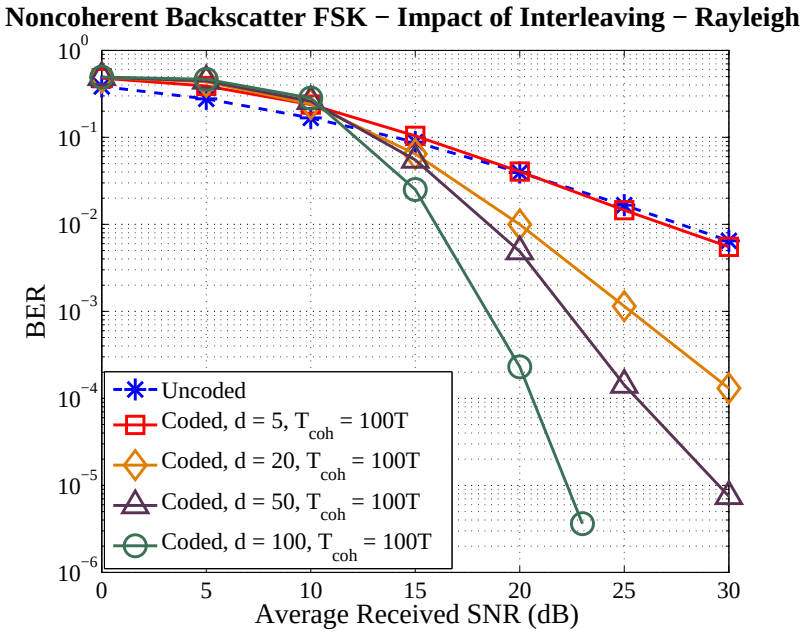


Figure 4.3: Impact of interleaving depth in BER performance of coded noncoherent bistatic scatter radio FSK with a $(32, 16, 8)$ RM channel code and fixed coherence time value $T_{\mathrm{coh}} = 100T$ seconds (with $K_{\mathrm{CT}} = K_{\mathrm{TR}} = 0$).

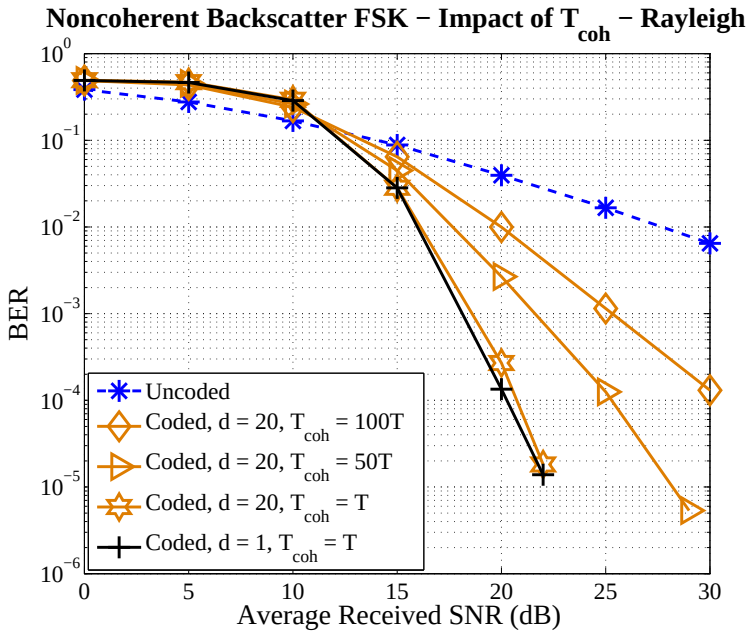


Figure 4.4: Impact of coherence time in BER performance of coded noncoherent bistatic scatter radio FSK with a $(32, 16, 8)$ RM channel code and fixed interleaving depth value (with $K_{\mathrm{CT}} = K_{\mathrm{TR}} = 0$).

the interleaving depth increases, the offered BER decreases. This happens because for fixed coherence time, $T_{\mathrm{coh}}$, the increase of the depth $d$ results to more independent coded bits per received codeword due to the reasons explained in Section 3.2. Hence, long bursts of errors in received codewords due to deep fading are avoided as $d$ increases. For the case where the interleaving depth equals the coherence time ($dT = T_{\mathrm{coh}}$) the coded system achieves full diversity through interleaving since each received symbol of each codeword undergoes independent fading. Specifically, for BER $= 10^{-2}$ the coded system with interleaving depths $d = 50$ and $d = 100$ offers 8dB and 11dB gain compared to noncoherent detection scheme. In the scenario of Fig. 4.4 we fix the value of interleaving depth to values $d = 1$, $d = 15$, whereas coherence time is altered. It is noted that as the coherence time decreases the BER decreases too. This happens because, every $T_{\mathrm{coh}}$ seconds, the channel coefficients of the links are independent, hence, for fixed interleaving depth the decrease of coherence time leads to more independent coded bits per codeword, and thus, the deep fading events are diminished. From Fig. 4.4 is noted that for $T_{\mathrm{coh}} = T$ (fast fading environment) the decoder without interleaving has similar BER performance to the decoder that utilizes $d = 20$.

Afterwards, the impact of CFO mismatch is considered for uncoded, as well as for coded

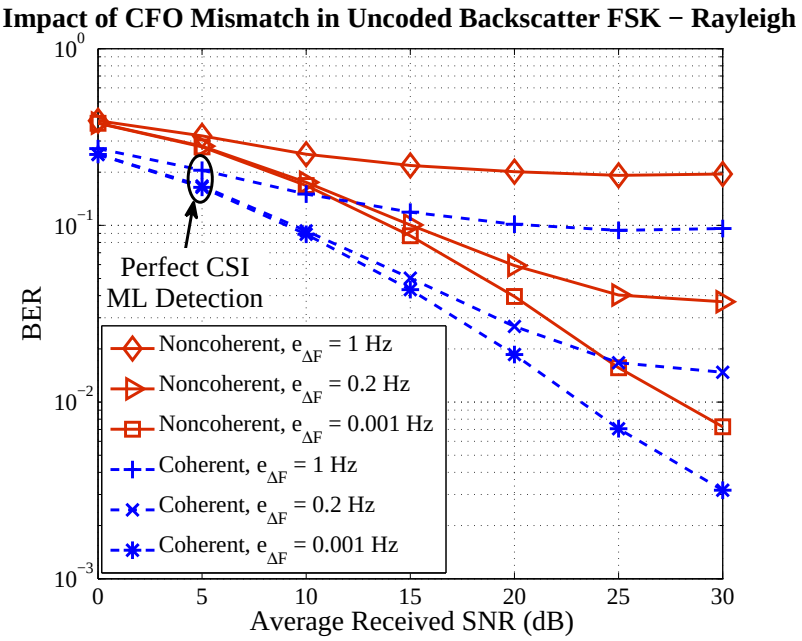


Figure 4.5: Impact of CFO estimation error $e_{\Delta F}$ in BER performance for uncoded noncoherent (Eq.(4.17)) and perfect CSI coherent [1] bistatic scatter radio FSK for fixed coherence time value (with $K_{\mathrm{CT}} = K_{\mathrm{TR}} = 0$).

noncoherent FSK. For the coded setup RM channel code $\mathcal{C}_{\mathrm{RM}}$ $(32, 16, 8)$ is considered and the decoding rule is given by Eq. (4.31). In such scenario, we define the following quantity

$$e_{\Delta F} \triangleq |\Delta F - \widehat{\Delta F}|,$$

which stands for the CFO estimation error. $\Delta F$ is the actual CFO, while $\widehat{\Delta F}$ is the estimated CFO. For the coded system, the parameters $T_{\mathrm{coh}}$ and $d$ were set to $T_{\mathrm{coh}} = 100T$ and $d = 20$. Fig. 4.5 presents the impact of CFO mismatch for noncoherent backscatter FSK (Eq. (4.28)) and coherent backscatter FSK with perfect channel state estimation (CSI) as presented in [1] and shows that their relative BER performance increases as the CFO estimation error increases. It is noted that for CFO estimation error $e_{\Delta F} = 1$ both schemes offer very poor BER performance. Fig. 4.6 compares noncoherent uncoded (Eq. (4.28)) and coded (Eq. (4.31)) systems with interleaving depth 20 while CFO estimation error alters. When $e_{\Delta F}$ is relative small the coded scheme performs better than the uncoded scheme for SNR values larger than 13dB. For high values of $e_{\Delta F}$ both schemes perform very poorly. Therefore, it is apparent that BER performance is significantly degraded as the CFO estimation error $e_{\Delta F}$ increases for all schemes. The figures related with CFO

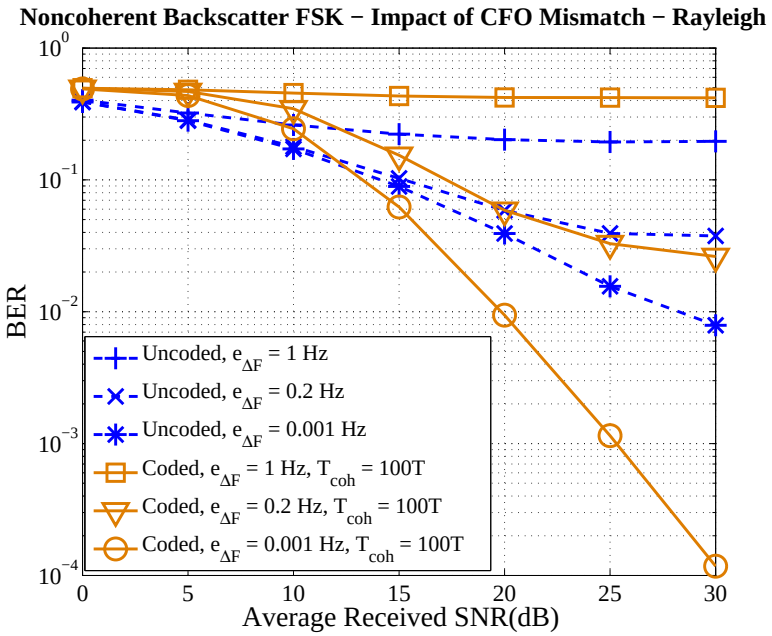


Figure 4.6: Impact of CFO mismatch in BER performance of uncoded (Eq.(4.17)) and coded (Eq. (4.31)) noncoherent bistatic scatter radio FSK with a $(32, 16, 8)$ RM channel code for fixed interleaving depth and coherence time value (with $K_{\mathrm{CT}} = K_{\mathrm{TR}} = 0$).

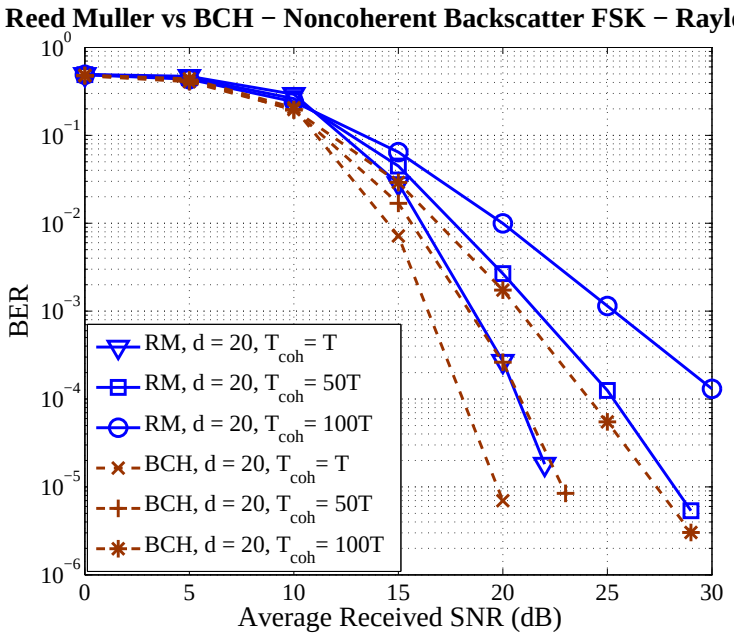


Figure 4.7: Comparison of $(32, 16, 8)$ RM code and $(31, 11, 11)$ BCH coded for noncoherent bistatic scatter radio FSK under the same assumptions (with $K_{\mathrm{CT}} = K_{\mathrm{TR}} = 0$).

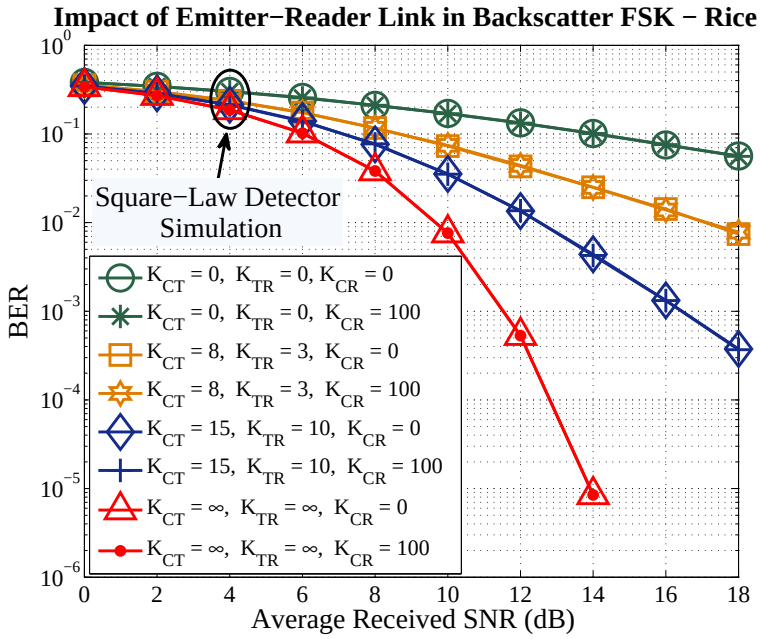


Figure 4.8: Comparison of square-law detector under different fading scenarios and different Rician $K_{\mathrm{CR}}$ values. The BER performance is not affected by carrier emitter-reader link.

mismatch highlight the importance of CFO estimation accuracy in the bistatic scatter radio FSK, and indicate that high frequency resolution should be employed in FFT periodogram at the receiver.

Finally, we consider the BER performance as a function of average received SNR for different coding schemes in bistatic scatter radio noncoherent FSK system for $T_{\mathrm{coh}} = 100T$. For channel coding the 2 following coding schemes are utilized:

- RM channel code $\mathcal{C}_{\mathrm{RM}}$ $(32, 16, 8)$ ,
- cyclic BCH channel code $\mathcal{C}_{\mathrm{BCH}}$ $(31, 11, 11)$.

Fig. 4.7 shows that BCH code has steeper BER curve than RM code, and thus, the former code achieves better coding gain. It is noted that $d_{\min}(\mathcal{C}_{\mathrm{RM}}) = 8 < 11 = d_{\min}(\mathcal{C}_{\mathrm{BCH}})$, thus, BCH code achieves better diversity order than RM code [23], and thus, the BER curve of the former code decreases faster, offering improved BER performance.

### Rician Fading

When the channel fading is Rician the BER curves decay more steeply. More specifically, Fig. 4.8 depicts the BER performance of uncoded system when the square-law detector

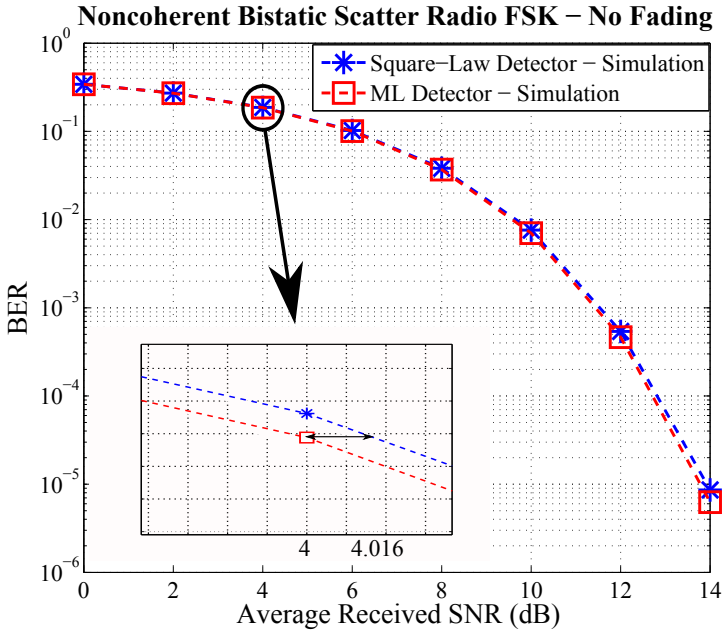


Figure 4.9: Comparison between ML detector (Eq. (4.13)) and square-law detector (Eq. (4.17)) over no fading channel ($K_{\mathrm{CT}} = K_{\mathrm{TR}} = \infty$).

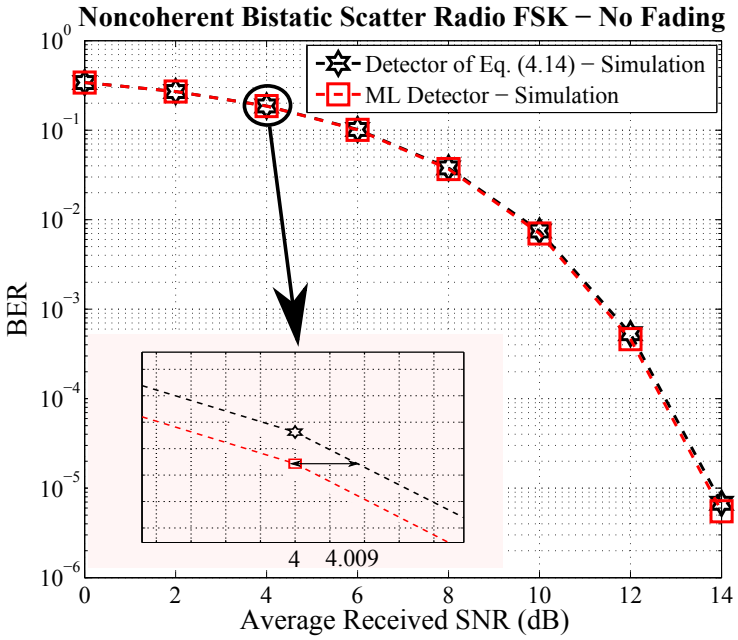


Figure 4.10: Comparison between ML detector (Eq. (4.13)) and near-ML detector (Eq. (4.14)) over no fading channel ($K_{\mathrm{CT}} = K_{\mathrm{TR}} = \infty$).

(Eq. (4.17)) is utilized for different kind of fading models. More importantly, the figure

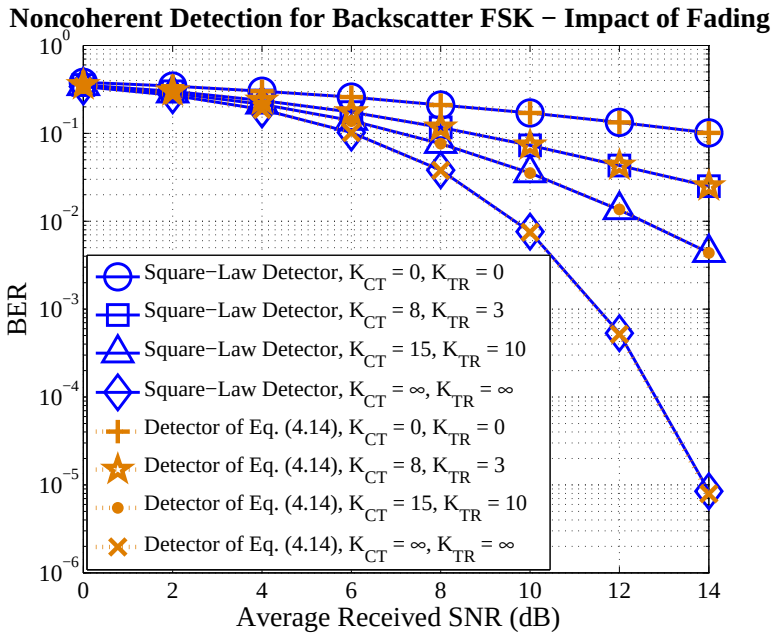


Figure 4.11: Comparison of square-law detector (Eq. (4.17)) and near-ML detector (Eq. (4.14)) over different types of Rician fading scenarios.

highlights that the BER performance does not alter when the fading type of carrier emitter-reader link changes, and thus, the BER performance does not depend on the reliability of carrier emitter-reader link, but on carrier emitter-tag-SDR reader compound link. From this figure is noted that as the Rician $K_l$ factor increases for any of the two links of interest, the offered BER decreases. Specifically, it is remarked that for BER $= 10^{-1}$ the SNR gap between Rayleigh fading ($K_{\mathrm{CT}} = K_{\mathrm{TR}} = 0$) and no fading ($K_{\mathrm{CT}} = K_{\mathrm{TR}} = \infty$) is approximately 8dB.

Figs. 4.9 and 4.11 compare the performance of ML detector of Eq. (4.13) with square-law detector (Eq. (4.17)), and with near-ML detector (Eq. (4.14)), respectively, when no fading is considered ($K_{\mathrm{CT}} = K_{\mathrm{TR}} = \infty$). On the former case the gap in terms of SNR is on the order of 0.02dB at low SNR regime and on the order of 0.2dB at high SNR regime. In the latter case the SNR gap is on the order of 0.01dB at low SNR regime and on the order of 0.15dB at high SNR regime. The above facts, constitute the detectors of Eqs (4.17) and (4.14) near-ML detectors in the case of $K_{\mathrm{CT}} = K_{\mathrm{TR}} = \infty$.

Fig. 4.11 compares the square-law detector (Eq (4.17)) and the detector of Eq (4.14) over different types of fading. It is observed that their BER performance is almost similar and their maximum gap is about 0.05dB. It is noted that the detector of Eq (4.14) achieves

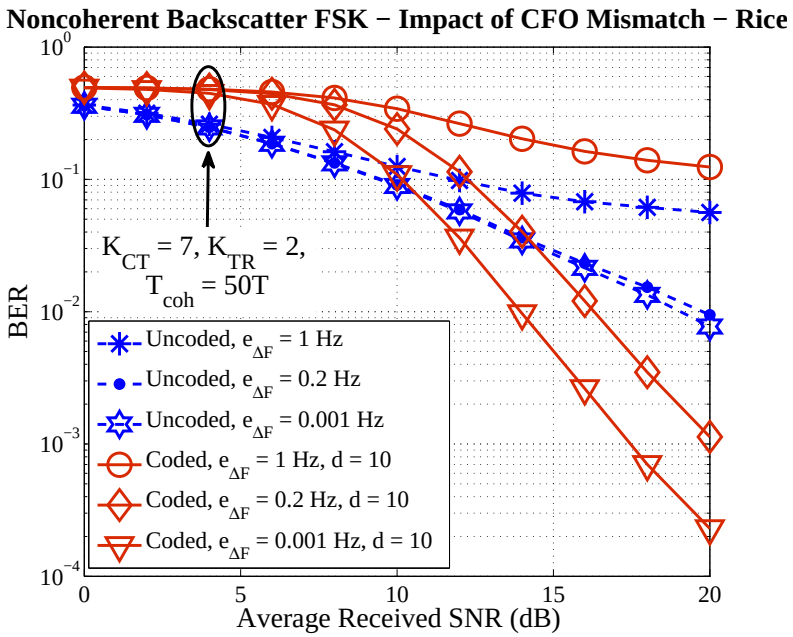


Figure 4.12: Impact of CFO estimation error in BER performance over Rician fading for noncoherent bistatic scatter radio FSK with uncoded system (Eq.(4.17)) and coded system (Eq. (4.31)) with a $(32, 16, 8)$ RM channel code for fixed coherence time value and interleaving depth.

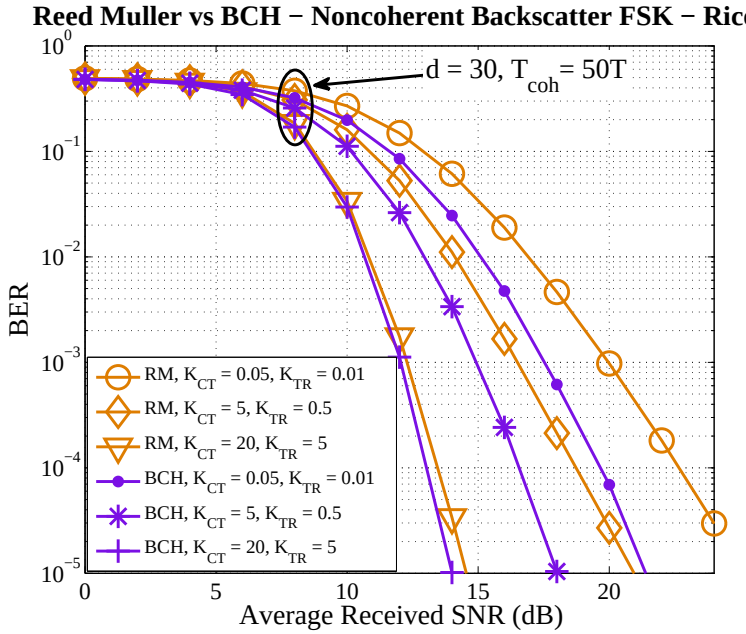


Figure 4.13: Comparison of $(32, 16, 8)$ RM code and $(31, 11, 11)$ BCH code for noncoherent bistatic backscatter FSK under the same assumptions over different Rician fading scenarios.

slightly better BER performance than square law detector for any SNR value and any Rician fading model.

Fig. 4.12 presents the impact of CFO estimation error $e_{\Delta F}$ for Rician fading with parameters $K_{\mathrm{CT}} = 7$ and $K_{\mathrm{TR}} = 2$. The BER performance of uncoded as well as coded system for different interleaving depth values is depicted. It is observed that for coherence time value $T_{\mathrm{coh}} = 50T$ and small CFO estimation error the depth 10 interleaving scheme offers improved BER performance due to the diversity gain through interleaving, since in such case portions of received codewords undergo independent fading. It is remarked that as the CFO estimation error increases the BER performance is degraded for any reception scheme. For $e_{\Delta F} = 1$Hz, all schemes perform very poorly.

Finally, Fig. 4.13 compares $\mathcal{C}_{\mathrm{RM}}\,(32, 16, 8)$ and $\mathcal{C}_{\mathrm{BCH}}\,(31, 11, 11)$ channel coding schemes over different Rician fading scenarios with $T_{\mathrm{coh}} = 50T$ and interleaving depth $d = 30$. It is remarked that BCH code offers improved BER performance compared to RM code for any considered Rician fading scenario. As Rician $K_{\mathrm{CT}}$ or $K_{\mathrm{TR}}$ factors increase the BER decreases for both coding schemes and the gap between them diminishes.

# Chapter 5

# Coherent Reception with Channel Coding in Bistatic Scatter Radio Link

Coherent receiver estimates the random parameters by means of maximum likelihood estimation. In order for the parameters to be estimated, the transmitter sends a known to receiver preamble bit sequence. After demodulation, the samples corresponding to the preamble sequence aid to estimate the random parameters. In such framework, the parameters are treated as constants for the estimation procedure, i.e. they are assumed to be nonrandom. The maximum likelihood estimation for the unknown parameters is obtained by the maximization (with respect to the parameters) of the log-likelihood pdf of the output given the known preamble sequence and the parameters. In this chapter only coherent OOK will be considered. Hereafter, the notation and the assumptions of Chapter 2 are adopted.[1]

## 5.1 Coherent Processing in OOK

### 5.1.1 Estimation of Random Parameters

The tag sends a sequence of $N_{\text{tr}}$ preamble bits along with a sequence of information bits, where the size of information sequence is not specified yet. The SDR reader after matched filtering has $N_{\text{tr}}$ observations corresponding to the preamble bits. Let $r_j$ for $j = 1, 2, \ldots, N_{\text{tr}}$, be the outputs of matched filter corresponding to the preamble sequence. Let $\mathcal{J}_0 \subset \{1, 2, \ldots, N_{\text{tr}}\}$ be the indexes of the preamble bits that correspond to bit "0", while, let $\mathcal{J}_1 = \{1, 2, \ldots, N_{\text{tr}}\} \backslash \mathcal{J}_0$ be the indexes of the preamble bits that correspond to

[1] Related results about coherent FSK in bistatic scatter radio framework can be found in [1, 33]

bit "1". We introduce the following hyperparameters

$$h \triangleq 2m_1 L\mathsf{e}^{-\mathrm{j}\phi_1} \in \mathbb{C},$$

and $A_{\mathrm{DC}}$ as defined in Subsection 2.1.2. These two compound hypeparameters incorporate 4 and 6 parameters (of the initial problem), respectively (specifically, they incorporate the parameters $\{a_l, \phi_l\},\ l \in \{\mathrm{CT}, \mathrm{TR}\}$ and $\{a_l, \phi_l\},\ l \in \{\mathrm{CR}, \mathrm{CT}, \mathrm{TR}\}$, respectively). In doing so, the parameter space is is reduced from $\mathbb{R}_+^3 \times [0, 2\pi)^3$ (see Eq. (3.2)) to $\mathbb{C}^2$. The output sequence corresponding to preamble bit sequence can be written as

$$r_j = A_{\mathrm{DC}} + hx_j + n_j, \quad j = 1, 2, \ldots, N_{\mathrm{tr}}, \quad x_j \in \{0, 1\}, \tag{5.1}$$

where the statistics of vector $n_j$ are defined as in Subsection 2.1.2. It is remarked that the output variables $r_j$ are conditionally independent each other for fixed transmitted sequence and hyperparameters. For the estimation of hyperparameter $A_{\mathrm{DC}}$ we utilize only the preamble bits corresponding to bit "0" (since the corresponding symbols do not depend on $h$) and thus, we obtain the following ML optimization problem

$$\begin{aligned}\widehat{A_{\mathrm{DC}}} &= \arg \max_{A_{\mathrm{DC}} \in \mathbb{C}} \mathsf{ln}\left(\prod_{j \in \mathcal{J}_0} f_{r_j|H_0, A_{\mathrm{DC}}}(r_j|H_0, A_{\mathrm{DC}})\right) \\ &= \arg \min_{A_{\mathrm{DC}} \in \mathbb{C}} \sum_{j \in \mathcal{J}_0} |r_j - A_{\mathrm{DC}}|^2 \Longrightarrow \widehat{A_{\mathrm{DC}}} = \frac{1}{|\mathcal{J}_0|} \sum_{j \in \mathcal{J}_0} r_j. \end{aligned} \tag{5.2}$$

The above optimization states that in order to estimate the DC-term it suffices to account only the preamble bits corresponding to bit "0", since when bit "0" is transmitted only a DC-term is scattered from the tag. After estimating $A_{\mathrm{DC}}$, the preamble bits corresponding to bit "1" are utilized in order to estimate the hyperparameter $h$, and thus, the ML optimization problem for $h$ is expressed as

$$\begin{aligned}\widehat{h} &= \arg \max_{h \in \mathbb{C}} \mathsf{ln}\left(\prod_{j \in \mathcal{J}_1} f_{r_j|H_1, A_{\mathrm{DC}}, h}(r_j|H_1, \widehat{A_{\mathrm{DC}}}, h)\right) \\ &= \arg \min_{h \in \mathbb{C}} \sum_{j \in \mathcal{J}_1} \left|(r_j - \widehat{A_{\mathrm{DC}}}) - h\right|^2 \Longrightarrow \widehat{h} = \frac{1}{|\mathcal{J}_1|} \sum_{j \in \mathcal{J}_1} r_j - \widehat{A_{\mathrm{DC}}}. \end{aligned} \tag{5.3}$$

### 5.1.2 Maximum Likelihood Coherent Detection

The receiver has estimated the hyperparameters $h$ and $A_{\rm DC}$ as discussed above, utilizing $N_{\rm tr}$ received observations corresponding to $N_{\rm tr}$ preamble bits and processes $N$ observations corresponding to $N$ transmitted bits (assuming no encoding). If we utilize the conditional independence of observations $r_j$ given the transmitted sequence and the hyperparameters $h$ and $A_{\rm DC}$, the optimal detection rule that minimizes the probability of bit error is written as follows (assuming equal priors for $H_0$ and $H_1$):

$$f_{r_j|H_0,A_{\rm DC},h}(r_j|H_0,\widehat{A_{\rm DC}},\widehat{h}) \underset{H_1}{\overset{H_0}{\gtrless}} f_{r_j|H_1,A_{\rm DC},h}(r_j|H_1,\widehat{A_{\rm DC}},\widehat{h}) \Longleftrightarrow$$
$$f_{r_j|H_0,A_{\rm DC}}(r_j|H_0,\widehat{A_{\rm DC}}) \underset{H_1}{\overset{H_0}{\gtrless}} f_{r_j|H_1,A_{\rm DC},h}(r_j|H_1,\widehat{A_{\rm DC}},\widehat{h}),\ j=1,2,\ldots,N.$$

That is, for given $\widehat{h}$ and $\widehat{A_{\rm DC}}$, the optimal (in term of bit error) coherent detection rule is the symbol-by-symbol detection. Thus, it is convenient to focus on a single bit period, hence, the subscripts can be omitted. Therefore, the ML detection rule is given by

$$f_{r|H_0,A_{\rm DC}}(r|H_0,\widehat{A_{\rm DC}}) \underset{H_1}{\overset{H_0}{\gtrless}} f_{r|H_1,A_{\rm DC},h}(r|H_1,\widehat{A_{\rm DC}},\widehat{h}) \Longleftrightarrow$$
$$\left|r-\widehat{A_{\rm DC}}\right|^2 \underset{H_0}{\overset{H_1}{\gtrless}} \left|\left(r-\widehat{A_{\rm DC}}\right)-\widehat{h}\right|^2 \Longleftrightarrow$$
$$2\Re\left\{\left(\widehat{h}\right)^*\left(r-\widehat{A_{\rm DC}}\right)\right\}-\left|\widehat{h}\right|^2 \underset{H_0}{\overset{H_1}{\gtrless}} 0 \Longleftrightarrow$$
$$\frac{2}{|\widehat{h}|}\Re\left\{\left(\widehat{h}\right)^*\left(r-\widehat{A_{\rm DC}}\right)\right\}-\left|\widehat{h}\right| \underset{H_0}{\overset{H_1}{\gtrless}} 0. \tag{5.4}$$

**BER Analysis for Rayleigh Fading** ($K_{\rm CT}=K_{\rm TR}=0$)

For simplicity, it is assumed that the receiver has perfect knowledge of the unknown hyperparameters, i.e. $\widehat{h}=h$ and $\widehat{A_{\rm DC}}=A_{\rm DC}$. In the following we analyze the probability of bit error of the ML detector of Eq.(5.4), when each link suffers from Rayleigh fading (i.e. parameters $a_{\rm CT}, a_{\rm TR}$ are Rayleigh distributed), i.e.,

$$f_{a_l}(x)=2x\mathsf{e}^{-x^2},\ x\geq 0,\quad l\in\{\rm CT,TR\}.$$

Firstly, the conditional probability of error given the parameters must be calculated. For given channel hyperparameter values $h$ and $A_{\rm DC}$, it is noted that under $H_0$: $r-A_{\rm DC}\sim$

$\mathcal{CN}(0, 2\sigma^2)$; while under $H_1$: $r - A_{\text{DC}} \sim \mathcal{CN}(h, 2\sigma^2)$ (where we set $\sigma^2 = \sigma_n^2 L$). Let

$$v \triangleq \frac{2}{|h|}\Re\left\{(h)^*\left(r - A_{\text{DC}}\right)\right\} - |h|. \tag{5.5}$$

Thus, for given hypothesis $H_0$ and hyperparameters $h$ and $A_{\text{DC}}$: $v \sim \mathcal{N}(-|h|, 4\sigma^2)$, while for given $H_1$, $h$ and $A_{\text{DC}}$: $v \sim \mathcal{N}(|h|, 4\sigma^2)$. Consequently, the detection problem of Eq. (5.4) can be rewritten as the following hypothesis testing problem (with equal priors)

$$\begin{aligned} H_0 &: v \sim \mathcal{N}(-|h|, 4\sigma^2) \\ H_1 &: v \sim \mathcal{N}(|h|, 4\sigma^2). \end{aligned}$$

The conditional probability of error of such hypothesis testing problem is known [34] and it's given by

$$\Pr(e|h) = \mathtt{Q}\left(\frac{|h|}{2\sigma}\right). \tag{5.6}$$

If we abbreviate

$$\begin{aligned} a &\triangleq a_{\text{CT}} a_{\text{TR}}, \\ \mu &\triangleq \frac{2m_1 L}{a}, \end{aligned}$$

we obtain that

$$|h| = \mu a. \tag{5.7}$$

If we use the definition of average received SNR for OOK modulation given by Eq.(2.28) we obtain

$$\mathtt{SNR} = \frac{s^2 P_C |\Gamma_0 - \Gamma_1|}{4\sigma_n^2} L = \frac{m_1^2 L^2}{8a^2\sigma_n^2 L} = \frac{\mu^2}{8\sigma^2} \Longrightarrow \frac{\mu}{\sigma} = 2\sqrt{2\mathtt{SNR}}. \tag{5.8}$$

Hence, the conditional probability of error given $h$ can be expressed as

$$\Pr(e|h) \overset{(5.6),(5.7)}{=} \mathtt{Q}\Big(a\frac{\mu}{2\sigma}\Big) \overset{(5.8)}{=} \mathtt{Q}\Big(a\sqrt{2\mathtt{SNR}}\Big) = \mathtt{Q}\Big(a_{\text{CT}} a_{\text{TR}}\sqrt{2\mathtt{SNR}}\Big) = \Pr(e|a_{\text{CT}}, a_{\text{TR}}). \tag{5.9}$$

Therefore the probability of bit error is obtained if we average the conditional probability

of bit error over the pdfs of r.v.'s $a_{\rm CT}$ and $a_{\rm TR}$,

$$\Pr(e) = \int_a \Pr(e|a) f_a(a) \mathsf{d}a = \int_x \int_y \Pr(e|a_{\rm CT}=x, a_{\rm TR}=y) f_{a_{\rm CT}}(x) f_{a_{\rm TR}}(y) \mathsf{d}x\mathsf{d}y$$
$$\overset{(5.9)}{=} \int_0^{+\infty} \int_0^{+\infty} \mathsf{Q}\Big(xy\sqrt{2\mathtt{SNR}}\Big) 4x^2y^2 \mathsf{e}^{-(x^2+y^2)} \mathsf{d}x\mathsf{d}y = \frac{1}{2} - \frac{\sqrt{\pi}}{4} \mathsf{U}\left(\frac{1}{2}, 0, \frac{1}{\mathtt{SNR}}\right), \quad (5.10)$$

where the following facts are utilized: (a) r.v's $a_{\rm CT}$ and $a_{\rm TR}$ are independent each other, (b) Eq. (6.287.2) from [26], and, (c) the definition of confluent hypergeomretric function U from Appendix (Eq. (A.10)).

### 5.1.3 Soft-Decision Maximum Likelihood Coherent Decoding

Firstly, it is assumed that no interleaving is utilized. Then, the ML decoder along with interleaving will be derived. The tag encodes a sequence of $K$ information bits into a sequence of $N$ coded bits (where $N$ stands for the codeword length), and appends a sequence of $N_{\rm tr}$ preamble bits at the start of the coded sequence. After matched filtering the SDR reader has a sequence of observations $\{r_j\}_{j=1}^{N+N_{\rm tr}}$. The receiver utilizes the first $N_{\rm tr}$ observations for synchronization and estimation of hyperparameters $\{h, A_{\rm DC}\}$, whereas the rest $N$ observation are utilized for soft-decision coherent ML decoding.

If we use the conditional independence of observations $r_j$ given the transmitted codeword and the hyperparameters $h$ and $A_{\rm DC}$, in conjunction with the ML decoding rule of Eq. (3.5), we obtain that

$$\mathbf{c}_{\rm ML} = \arg\max_{\mathbf{c}\in\mathcal{C}} \prod_{j=1}^{N} f_{r_j|\mathbf{c},A_{\rm DC},h}(r_j|\mathbf{c}, \widehat{A_{\rm DC}}, \widehat{h}) = \arg\max_{\mathbf{c}\in\mathcal{C}} \prod_{j=1}^{N} f_{r_j|c_j,A_{\rm DC},h}(r_j|c_j, \widehat{A_{\rm DC}}, \widehat{h})$$
$$= \arg\max_{\mathbf{c}\in\mathcal{C}} \mathsf{ln}\left(\prod_{j=1}^{N} f_{r_j|c_j,A_{\rm DC},h}(r_j|c_j, \widehat{A_{\rm DC}}, \widehat{h})\right)$$
$$= \arg\max_{\mathbf{c}\in\mathcal{C}} \mathsf{ln}\left(\prod_{j=1}^{N} \Big(f_{r_j|H_0,A_{\rm DC}}(r_j|H_0, \widehat{A_{\rm DC}})\Big)^{1-c_j} \Big(f_{r_j|H_1,A_{\rm DC},h}(r_j|H_1, \widehat{A_{\rm DC}}, \widehat{h})\Big)^{c_j}\right)$$
$$= \arg\min_{\mathbf{c}\in\mathcal{C}} \sum_{j=1}^{N} \left(\frac{1-c_j}{2\sigma^2}\right) \left|r_j - \widehat{A_{DC}}\right|^2 + \left(\frac{c_j}{2\sigma^2}\right) \left|r_j - \widehat{A_{DC}} - \widehat{h}\right|^2$$
$$= \arg\max_{\mathbf{c}\in\mathcal{C}} \sum_{j=1}^{N} c_j \left(\Re\left\{\left(\widehat{h}\right)^* \left(r_j - \widehat{A_{\rm DC}}\right)\right\} - 0.5\left|\widehat{h}\right|^2\right), \quad (5.11)$$

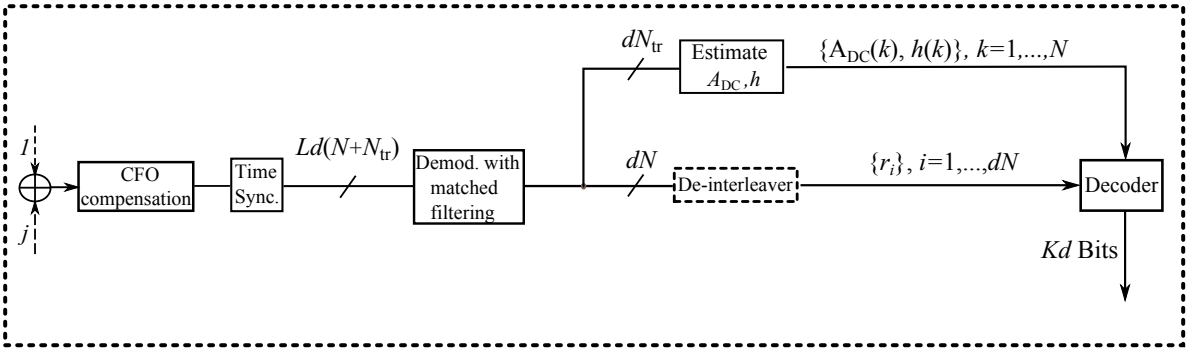


Figure 5.1: Complete signal processing chain with channel coding for coherent OOK in bistatic backscatter radio.

where $c_j$ denotes the $j$th element of codeword $\mathbf{c}$.

If the channel coherence time is known and the system is delay tolerant then an interleaver can be utilized in conjunction with channel coding. The transmitter utilizes an interleaver whose depth and training sequence duration is equal to the coherence time, i.e. $dT+N_{\text{tr}}T = T_{\text{coh}}$. The receiver for each block of $d+N_{\text{tr}}$ bits (for every column) assumes that the channel remains flat and estimates the parameters $h$ and $A_{\text{DC}}$ based on preamble bits and forms the following parameters: $\left\{\widehat{h}(k), \widehat{A_{\text{DC}}}(k)\right\}_{k=1}^{N}$. The received observations after de-interleaving are in such way, such that, observations $r_j$, $j = 1, 2, \ldots, dN$, correspond to $d$ consecutive codewords. For fixed transmitted codeword, and fixed $\left\{\widehat{h}(k), \widehat{A_{\text{DC}}}(k)\right\}_{k=1}^{N}$, every $N$ observations corresponding to a codeword have conditionally independent elements, and furthermore, each element undergoes independent fading, hence, the ML decoder for depth $d$ interleaving can be written as follows ($i = 1, 2, \ldots, d$)

$$\begin{aligned}
\mathbf{c}_{\text{ML}}(i) &= \arg\max_{\mathbf{c}\in\mathcal{C}} \prod_{k=1}^{N} f_{r_{(i-1)N+k}|\mathbf{c},A_{\text{DC}}(k),h(k)}(r_{(i-1)N+k}|\mathbf{c}, \widehat{A_{\text{DC}}}(k), \widehat{h}(k)) \\
&= \arg\max_{\mathbf{c}\in\mathcal{C}} \ln\Bigg( \prod_{k=1}^{N} \left(f_{r_{(i-1)N+k}|H_0,A_{\text{DC}}(k)}(r_{(i-1)N+k}|H_0, \widehat{A_{\text{DC}}}(k))\right)^{1-c_j} \times \\
&\times \left(f_{r_{(i-1)N+k}|H_1,A_{\text{DC}}(k),h(k)}(r_{(i-1)N+k}|H_1, \widehat{A_{\text{DC}}}(k), \widehat{h}(k))\right)^{c_j} \Bigg) \\
&= \arg\max_{\mathbf{c}\in\mathcal{C}} \left\{ \sum_{k=1}^{N} c_k \left( \Re\left\{ \left(\widehat{h}(k)\right)^{*} \left(r_{(i-1)N+k} - \widehat{A_{\text{DC}}}(k)\right)\right\} - 0.5\left|\widehat{h}(k)\right|^2 \right) \right\},
\end{aligned} \tag{5.12}$$

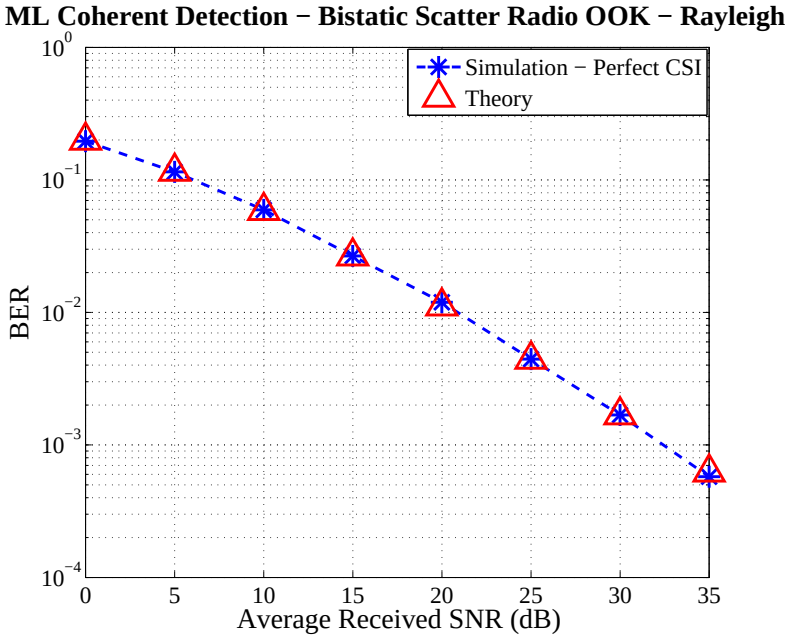


Figure 5.2: BER performance as a function of SNR of uncoded coherent bistatic scatter radio OOK over Rayleigh fading ($K_{\mathrm{CT}} = K_{\mathrm{TR}} = 0$). Simulation results match perfectly with analytical results.

where $\mathbf{c}_{\mathrm{ML}}(i)$ denotes the $i$th estimated codeword out of $d$. The whole signal processing chain for coherent bistatic scatter radio OOK is illustrated in Fig. 5.1.

### 5.1.4 Simulation Results

Simulation results are carried out for bistatic scatter radio system utilizing coherent OOK modulation for uncoded as well as for coded system. It is assumed that each link suffers from Rayleigh fading (i.e. $K_{\mathrm{CT}} = K_{\mathrm{TR}} = 0$).[2] The impact of several communication parameters in BER performance is presented for such scenario. In all simulation results the parameters CSR and oversampling factor ($L$) are set 20dB and 100 samples per bit, respectively. For the simulation results regarding coding setup, a $(32, 16, 8)$ RM channel code is considered with an energy budget constraint discussed in Subsection 4.1.3.

For the uncoded setup, Fig. 5.2 shows the simulated and analytical BER performance of the OOK detector of Eq. (5.4) as a function of average received SNR, SNR of Eq. (2.28). We note that the analytical BER performance of Eq. (5.10) matches perfectly with simulation

[2]The uncoded scheme in the figures of Rayleigh fading scenario correspond to the ML coherent detector (Eq. (5.4)).

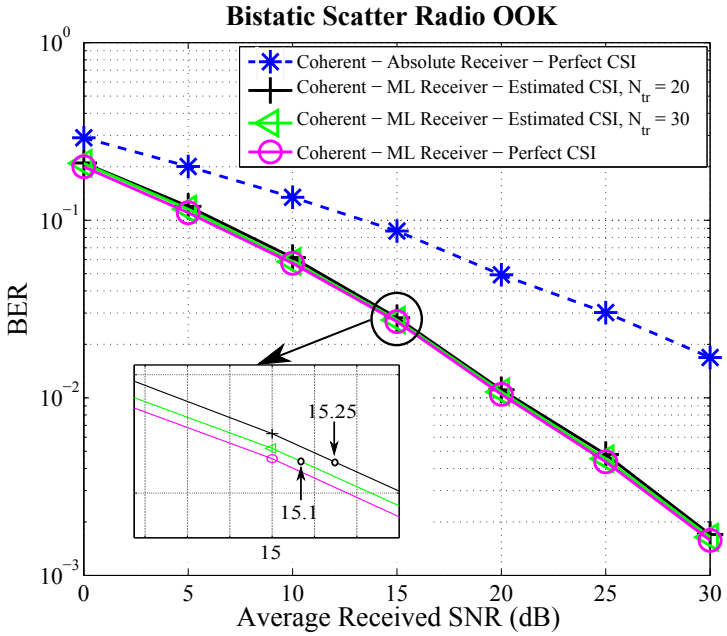


Figure 5.3: BER performance comparison of the system with perfect CSI and the system with estimated CSI using preample sequence for coherent bistatic scatter radio OOK (with $K_{\mathrm{CT}} = K_{\mathrm{TR}} = 0$).

results. The proposed receiver is compared with the absolute receiver (dashed curve) proposed in [13] which utilizes an absolute operation on the received waveform before the processing. In doing so, the need of CFO estimation is totally eliminated; on the other hand, the absolute operation loses at least 3dB in BER performance. From Fig. 5.2 is noted that as the SNR increases the gap in BER performance among the 2 schemes is also increased. We observe that at BER $= 0.2$ the gap is 5dB, while at BER $= 10^{-2}$ the gap is larger than 10dB. It is remarked that for these simulation results perfect CFO estimation is assumed. The impact of CFO mismatch on the ML receivers is discussed subsequently.

Fig. 5.3 depicts the BER performance loss for uncoded system which utilizes the ML detection rule of Eq (5.4) when the parameters $\{h, A_{\mathrm{DC}}\}$ are estimated through Eqs. (5.3) and (5.2), respectively. It is noted that for 20 and 30 training symbols preamble for parameter estimation, the performance loss is approximately 0.25dB and 0.1dB compared to perfect CSI scheme, respectively.

Fig. 5.4 depicts the impact of interleaving when coding is utilized. It is noted that for fixed value of coherence time $T_{\mathrm{coh}} = 100T$ the BER decreases as interleaving depth increases. This fact corroborates the results discussed in Section 3.2.

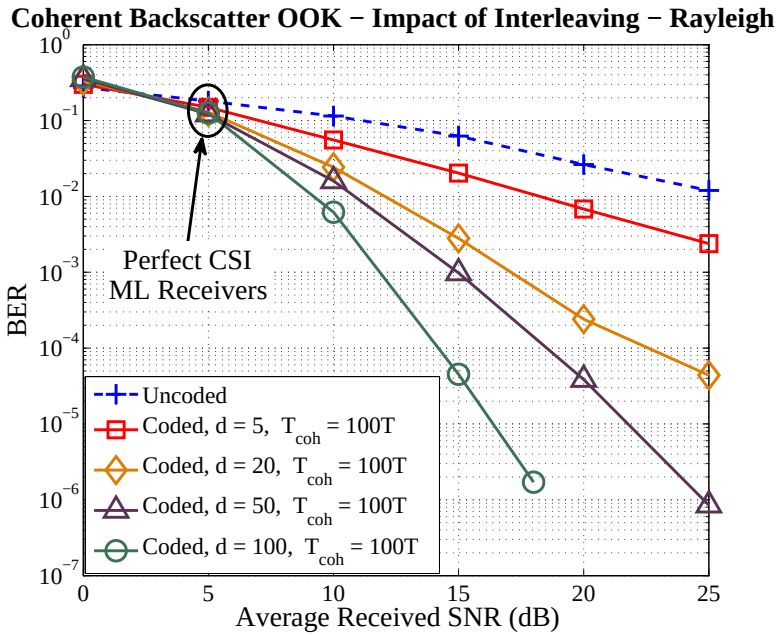


Figure 5.4: Impact of interleaving depth in BER performance of perfect CSI coded coherent bistatic scatter radio OOK with a $(32, 16, 8)$ RM channel code and fixed coherence time value $T_{\text{coh}} = 100T$ seconds (with $K_{\text{CT}} = K_{\text{TR}} = 0$).

Afterwards, we combine the above results and present the BER performance for coded scheme along with different interleaving depths when the receiver estimates $\{h, A_{\text{DC}}\}$ through Eqs. (5.3), (5.2) and when the receiver has perfect CSI. It is noted that with 40 training bits for parameter estimation, the maximum performance loss is approximately 0.8dB, and thus, the effectiveness of the proposed ML estimation is verified.

Finally, the impact of CFO mismatch is addressed in Fig. 5.6 for uncoded, as well as for coded coherent OOK with parameter values $\texttt{CSR} = 20$dB, $L = 100$ and $T_{\text{coh}} = 100T$ and perfect CSI at the receiver for all schemes. The parameter $e_{\Delta F}$ is defined as in Subsection 4.1.3. Fig. 5.6 shows the comparison of uncoded and coded coherent OOK when the CFO estimation error changes. It is noted that OOK modulation is more sensitive in CFO estimation errors than FSK and offers larger BER performance degradation when CFO estimation error increases. Hence, ultra high frequency resolution in FFT periodogram is prerequisite for good BER performance. The dot curve shows the performance of uncoded absolute receiver which is unchanged due to its CFO estimation error invariance. Therefore, when the receiver cannot afford high frequency resolution the utilization of absolute receiver is more convenient.

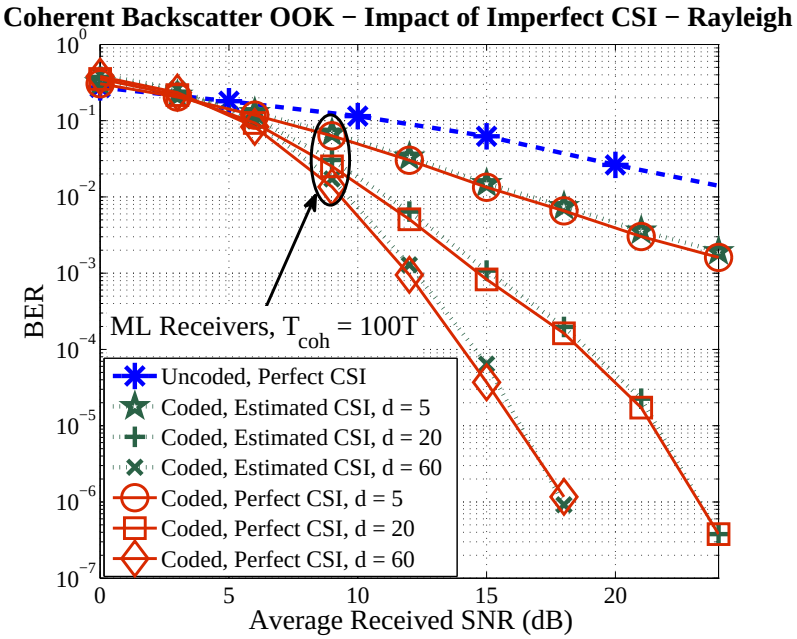


Figure 5.5: BER performance comparison of the system with perfect CSI and the system with estimated CSI using preamble sequence for coherent coded bistatic scatter radio OOK with a $(32, 16, 8)$ RM channel code and fixed coherence time value $T_{\text{coh}} = 100T$ seconds (with $K_{\text{CT}} = K_{\text{TR}} = 0$).

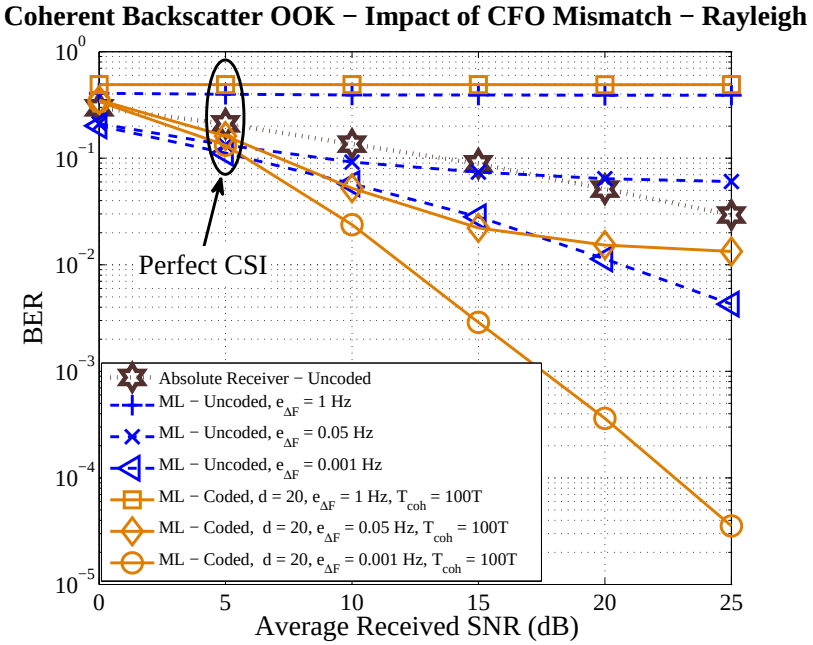


Figure 5.6: BER performance degradation due to CFO estimation error $e_{\Delta F}$ for perfect CSI uncoded and coded coherent bistatic scatter radio OOK with a $(32, 16, 8)$ RM channel code with fixed values for interleaving depth and coherence time (with $K_{\text{CT}} = K_{\text{TR}} = 0$).

# Chapter 6

# Experimental Results

## 6.1 Experimental Results

Ranging measurements were conducted outdoors. A carrier emitter was utilized with +13dBm transmission power at 867MHz. A programmable, semi-passive RF tag (based on a 8-bit ultra-low power micro-controller unit from Silicon Laboratories) was used to modulate the reflected carrier with FSK modulation at 1kbps bit-rate. Reception was implemented with a commodity USRP1 software defined radio (SDR) and a laptop PC, running the decoding reception scheme proposed in [20] for the coded setup, and the reception scheme from [13] for the uncoded setup. Omnidirectional antennas were employed on both emitter, tag and SDR reader. For the uncoded setup, a packet of 62 preamble bits


Figure 6.1: Bistatic experimental setup for backscatter radio.

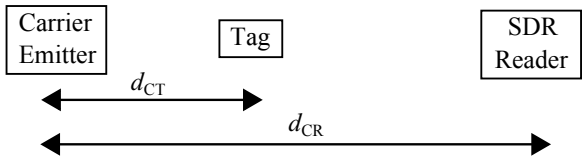


Figure 6.2: Scenario 1: Tag between carrier emitter and reader.

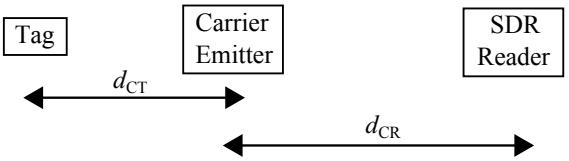


Figure 6.3: Scenario 2: Carrier emitter between tag and reader.

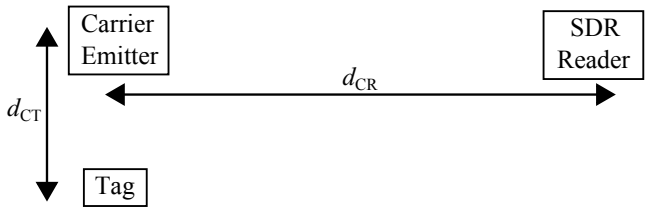


Figure 6.4: Scenario 3: 90 degrees angle between tag - carrier emitter and carrier emitter - reader.

(known to receiver for synchronization) plus 32 information bits was utilized, whereas for the coded setup, the packet consisted of 62 preamble bits plus 64 coded bits. The coded system employed a $(32, 16, 8)$ Reed-Muller code with interleaving depth $d = 2$.

Three different scenarios were studied, depicted at Figs. 6.2, 6.3, 6.4. In scenario 1, tag was located between carrier emitter and reader (Fig. 6.2), in scenario 2, the carrier emitter was placed between tag and reader, so that the tag-to-reader distance was larger than emitter-to-reader distance (Fig. 6.3). Finally, in scenario 3 the tree terminals formed a rectangle (Fig. 6.4).

Table 6.1 offers the achieved ranges from the experimental tests (Fig. 6.1); it is found that for the specific setup, the offered tag-to-reader ranges can be increased by at least 6 meters for scenario 1 and 14 meters for scenario 3, using the low-complexity, small block-length channel codes with the proposed simple decoder. Equivalently, for similar ranges, the proposed processing with channel coding offers more reliable communication, compared to the uncoded case, as expected. In fact, ranges on the order of hundreds of meters are feasible, corroborating the idea of bistatic backscatter radio for wireless sensor network applications; a large number of stochastically-placed emitters, potentially power through

Table 6.1: BER performance for different scenarios

| Scenario | $d_{\mathrm{CR}}$ | $d_{\mathrm{CT}}$ | $d_{\mathrm{TR}}$ | BER coded | BER uncoded |
|---|---|---|---|---|---|
| 1 | 134 m | 2.8 m | **131.2** m | 3.03% | $> 15\%$ |
| 1 | 128 m | 2.8 m | **125.2** m | 0% | 6.4% |
| 2 | 128 m | 4.8 m | **132.8** m | 3.24% | 12.11% |
| 3 | 134 m | 2.6 m | **134.025** m | 5.07% | $> 15\%$ |
| 3 | 120.4 m | 2.6 m | **120.43** m | 0% | 8.04% |

energy harvesting techniques could illuminate a sheer number of tags that reflect their signals towards one (or more) SDR readers. In that way, a large geographical area can be served and this work is a small step forward towards the realization of that vision.

# Chapter 7

# Conclusion

The bistatic scatter radio system was presented, which can be harnessed to design flexible, ultra low-cost, low-power, large scale sensor networks (WSNs) with extended field coverage. Inherent problems of bistatic architecture are also discussed and solutions are provided. Although, bistatic scatter radio has peculiar signal model with several inherent microwave and communication parameters, this work effectively employed low-complexity noncoherent (for FSK) and coherent (for OOK) reception schemes over Rician and Rayleigh fading environments, respectively. Efficient small block length channel codes are proposed for bistatic setup with ultra low-complexity encoding, ideal for resource constraint tags.

For first time in scatter radio-related literature, this work proposed composite hypothesis testing decoding rule for noncoherent bistatic backscatter FSK that adheres to a very simple optimization problem. Moreover, the equivalence of square-law FSK detector with the composite hypothesis detection rule is shown. Efficient low-complexity channel estimation procedure for coherent OOK is proposed and ML detection/decoding rules are derived.

Simulation results clarified the impact of several communication parameters that affect the BER performance of the FSK/OOK systems and revealed complexity–accuracy trade-offs. Especially, FSK modulation is a practical option for wireless sensor networking scenarios operating in power-limited regime and allows for simple frequency division multiple access of simultaneously receiver-less RF tags. Consequently, by focusing in noncoherent FSK, we characterized the effective range gains of the noncoherent detection/decoding schemes proposed in [20] through experimental measurements which conducted outdoors in an open field. A custom carrier emitter was set to transmit a sinusoid wave with 13 dBm transmit power, illuminating a custom RF tag. A USRP-1 software defined radio connected to a laptop running custom receiver scripts was receiving the backscattered signal from tag. Experimental ranges on the order of 100 meters were demonstrated with omnidirectional antennas and 13 dBm transmission power.

In conclusion, the proposed receivers offer a practical solution that could lead to the adoption of bistatic scatter radio in low-power, low-cost, large scale WSNs.

# Appendix A

# Useful Function Formulas

In this chapter we offer some special functions that we encounter in this thesis. For an integrated exposition the reader is referred to [35]

## A.1 Gamma Function

Gamma function $\Gamma(\cdot)$ is defined on complex numbers except the negative integers and zero

$$\Gamma(x) = \int_0^\infty t^{x-1}\mathsf{e}^{-t}\mathsf{d}t, \quad x \in \mathbb{C}\backslash\{i \in \mathbb{Z} : i \leq 0\}. \tag{A.1}$$

When $x \in \mathbb{N}$ then

$$\Gamma(x) = (x-1)! \tag{A.2}$$

## A.2 Exponential Integral Function

For real nonzero values of $x$, the exponential integral $\mathsf{Ei}(x)$ is defined as

$$\mathsf{Ei}(x) = -\int_{-x}^\infty \frac{\mathsf{e}^{-t}}{t}\mathsf{d}t, \quad x \in \{y \in \mathbb{R} : y \geq 0\}. \tag{A.3}$$

## A.3 Incomplete Upper Gamma Function

The upper incomplete function is defined as

$$\Gamma(s,x) = \int_x^\infty t^{s-1}\mathsf{e}^{-t}\mathsf{d}t, \quad s \in \{y \in \mathbb{C} : \Re\{y\} \geq 0\}, \quad x \in \mathbb{C}. \tag{A.4}$$

When $s = 0$ and $x > 0$ then

$$\Gamma(0,x) = -\mathsf{Ei}(-x). \tag{A.5}$$

## A.4 Modified Bessel Functions

### A.4.1 Modified Bessel Function of First Kind

If we restrict the parameters $\nu$ and $x$ to be real numbers the modified Bessel function of first kind is given as

$$\mathsf{I}_\nu(x) = \left(\frac{x}{2}\right)^\nu \sum_{k=0}^{+\infty} \frac{\left(\frac{x}{2}\right)^{2k}}{k!\,\Gamma(\nu+k+1)}, \quad \nu, x \in \mathbb{R} \tag{A.6}$$

### A.4.2 Modified Bessel Function of Second Kind

The modified Bessel function of second kind is defined as

$$\mathsf{K}_\nu(x) = \left(\frac{\pi}{2}\right) \frac{\mathsf{I}_{-\nu}(x) - \mathsf{I}_\nu(x)}{\mathsf{sin}(\nu\pi)}, \quad \nu, x \in \mathbb{R}. \tag{A.7}$$

In special case of $\nu = 0$ and $x > 0$ we have that

$$\mathsf{K}_0(x) = \int_0^{+\infty} \mathsf{cos}\left(x\mathsf{sinh}(t)\right) \mathsf{d}t. \tag{A.8}$$

## A.5 Q-Function

Q-function is widely used in telecommunication application and it is usually utilized for probability of error expressions. It is defined as follows

$$\mathsf{Q}(x) = \frac{1}{2\pi} \int_x^{\infty} \mathsf{e}^{-\frac{t^2}{2}} \mathsf{d}t, \quad x \in \mathbb{R}. \tag{A.9}$$

## A.6 Confluent Hypergeometric function U

For $a > 0$ and $b > 0$ the confluent hypergeometric function U is given be the following formula

$$\mathsf{U}(a, b, x) = \frac{1}{\Gamma(a)} \int_0^{+\infty} \mathsf{e}^{-xt} t^{a-1} (1+t)^{b-a-1} \mathsf{d}t, \quad x \in \mathbb{C}. \tag{A.10}$$

# Bibliography

[1] N. Fasarakis-Hilliard, P. N. Alevizos, and A. Bletsas, "Coherent detection and channel coding for bistatic scatter radio sensor networking," *IEEE Trans. Commun.*, submitted.

[2] I. F. Akyildiz, W. Su, Y. Sankarasubramaniam, and E. Cayirci, "Wireless sensor networks: A survey," *Comput. Netw.*, vol. 38, no. 4, pp. 393–422, Mar. 2002.

[3] H. Stockman, "Communication by means of reflected power," in *Proc. IRE*, Oct. 1948, pp. 1196–1204.

[4] G. Vannucci, A. Bletsas, and D. Leigh, "A software-defined radio system for backscatter sensor networks," *IEEE Trans. Wireless Commun.*, vol. 7, no. 6, pp. 2170–2179, Jun. 2008.

[5] V. Lakafosis, A. Rida, R. Vyas, L. Yang, S. Nikolaou, and M. M. Tentzeris, "Progress towards the first wireless sensor networks consisting of inkjet-printed, paper-based RFID-enabled sensor tags," *Proc. IEEE*, vol. 98, no. 9, pp. 1601–1609, Sep. 2010.

[6] E. Kampianakis, J. Kimionis, K. Tountas, C. Konstantopoulos, E. Koutroulis, and A. Bletsas, "Wireless environmental sensor networking with analog scatter radio & timer principles," *IEEE Sensors J.*, vol. 14, no. 10, pp. 3365–3376, Oct. 2014.

[7] J. Virtanen, L. Ukkonen, T. Björninen, A. Z. Elsherbeni, and L. Sydänheimo, "Inkjet-Printed Humidity Sensor for Passive UHF RFID Systems," *IEEE Trans. Instrum. Meas.*, vol. 60, no. 8, pp. 2768–2777, Aug. 2011.

[8] C. Angerer, R. Langwieser, and M. Rupp, "RFID reader receivers for physical layer collision recovery," *IEEE Trans. Commun.*, vol. 58, no. 12, pp. 3526–3537, Dec. 2010.

[9] J. D. Griffin and G. D. Durgin, "Complete link budgets for backscatterradio and RFID systems," *IEEE Antennas Propag. Mag.*, vol. 51, no. 2, pp. 11–25, Apr. 2009.

[10] D. Kim, M. A. Ingram, and W. W. Smith Jr., "Measurements of small-scale fading and path loss for long range RF tags," *IEEE Trans. Antennas Propagat.*, vol. 51, no. 8, pp. 1740–1749, Aug. 2003.

[11] A. Collado and A. Georgiadis, "Conformal Hybrid Solar and Electromagnetic (EM) Energy Harvesting Rectenna," *IEEE Trans. Circuits Syst. I*, vol. 60, pp. 2225–2234, Aug. 2013.

[12] A. Bletsas, S. Siachalou, and J. N. Sahalos, "Anti-collision backscatter sensor networks," *IEEE Trans. Wireless Commun.*, vol. 8, no. 10, pp. 5018–5029, Oct. 2009.

[13] J. Kimionis, A. Bletsas, and J. N. Sahalos, "Increased range bistatic scatter radio," *IEEE Trans. Commun.*, vol. 62, no. 3, pp. 1091–1104, Mar. 2014.

[14] ——, "Design and implementation of RFID systems with software defined radio," in *Proc. IEEE European Conf. on Antennas and Propagation (EuCAP)*, Prague, Czech Republic, Mar. 2012, pp. 3464–3468.

[15] ——, "Bistatic backscatter radio for power-limited sensor networks," Atlanta, GA, USA, Dec. 2013, pp. 353–358.

[16] J. Kimionis, "Bistatic scatter radio for increased-range environmental sensing," Master's thesis, Technical University of Crete, Aug. 2013, supervisor A. Bletsas.

[17] E. Kampianakis, "Scatter radio sensor network with analog frequency modulation principles," Master's thesis, Technical University of Crete, Jul. 2014, supervisor A. Bletsas.

[18] C. Shannon, "A mathematical theory of communication," *Bell System Technical Journal*, vol. 27, pp. 379–423, 623–656, 1948.

[19] R. G. Gallager, *Information Theory and Reliable Communication*. New York, NY, USA: John Wiley & Sons, Inc., 1968.

[20] P. N. Alevizos, N. Fasarakis-Hilliard, K. Tountas, N. Agadakos, N. Kargas, and A. Bletsas, "Channel coding for increased range bistatic backscatter radio: Experimental results," in *Proc. IEEE RFID Technology and Applications (RFID-TA)*, Tampere, Finland, Sep. 2014.

[21] A. Bletsas, A. G. Dimitriou, and J. N. Sahalos, "Improving backscatter radio tag efficiency," *IEEE Trans. Microwave Theory Tech.*, vol. 58, no. 6, pp. 1502–1509, Jun. 2010.

[22] S. Thomas, E. Wheeler, J. Teizer, and M. Reynolds, "Quadrature amplitude modulated backscatter in passive and semipassive UHF RFID systems," *IEEE Trans. Microwave Theory Tech.*, vol. 60, no. 4, pp. 1175–1182, Apr. 2012.

[23] J. G. Proakis and M. Salehi, *Digital Communications*, 5th ed. Upper Saddle River, NJ, USA: Prentice-Hall, November 2007.

[24] R. Gallager, *Principles of Digital Communication.* Cambridge University Press, 2008.

[25] A. Papoulis and S. U. Pillai, *Probability, Random Variables, and Stochastic Processes*, 4th ed. McGraw-Hill Higher Education, 2002.

[26] I. S. Gradshteyn and I. M. Ryzhik, *Table of integrals, series, and products*, 7th ed. Elsevier/Academic Press, Amsterdam, 2007.

[27] T. Richardson and R. Urbanke, *Modern Coding Theory.* Cambridge University Press, 2008.

[28] T. K. Moon, *Error Correction Coding: Mathematical Methods and Algorithms.* Wiley-Interscience, 2005.

[29] S. Lin and D. J. Costello, *Error Control Coding* , 2nd ed. Prentice Hall, Jun. 2004.

[30] J. G. Proakis and M. Salehi, *Communication Systems Engineering*, 2nd ed. Upper Saddle River, NJ, USA: Prentice-Hall, August 2001.

[31] D. J. Costello and G. D. Forney Jr., "Channel coding: The road to channel capacity," *Proc. IEEE*, vol. 95, no. 6, pp. 1150 – 1177, Jun. 2007.

[32] G. D. Forney Jr., "Introduction to binary block codes," MIT, 2005, principles of Digital Communication II.

[33] N. Fasarakis-Hilliard, "Coherent detection and channel coding for backscatter sensor networks," Master's thesis, Technical University of Crete, Aug. 2014, supervisor A. Bletsas.

[34] B. C. Levy, *Principles of Signal Detection and Parameter Estimation*. New York: Springer, 2008.

[35] F. W. J. Olver, D. W. Lozier, R. F. Boisvert, and C. W. Clark, *NIST handbook of mathematical functions*. New York, NY: Cambridge Univ. Press, 2010.